Response to Anonymous Referee #4

We thank the reviewer for their valuable comments. Throughout the document reviewer comments are displayed in standard font while author responses are presented with blue text.

This work details a set of pseudo-data experiments in which the prior flux and prior flux uncertainty are varied in a systematic manner in order to assess the sensitivity of atmospheric inversions with satellite data to the prior flux constraint. The manner in which this is carried out is a good template for assessing sensitivity to inversion system ingredients.

General comments: 1. The presentation in terms of images makes some of the conclusions and discussion difficult to assess. Specifically I'm referring to Figures 3-5, where the "meat" of the results is contained. I would suggest that the NEE range differences are great material for a table, and that the other two columns are perfect to be condensed into stacked bars or something similar for ease of visibility.

We appreciate the comment from the reviewer regarding Fig. 3-5 in the original manuscript (now Fig. 6-8 of the updated version of the manuscript). While producing the manuscript we spent significant time and effort developing these figures in order to present as much information as possible in a clear manner. Due to the large amount of information provided in these figures, it proved a difficult task. We tested numerous figure types (line graphs, stacked bar graphs, pie charts, etc.) and determined the current layout was the most effective. Specifically, for the stacked bar charts, when multiple prior or posterior NEE estimates are very similar (which happens frequently) for a specific region/season, they will not be visible as there is not enough difference in the values. After numerous versions of Fig. 3-5 we reverted back to the grouped bar chart format as the best way to display the main results of this study.

We point the reviewer to Table 3 of the manuscript where NEE range values illustrated in Fig. 6 are already listed (along with "true", multi-model prior and posterior means, and standard deviations of NEE values shown in Fig. 6). We have added the following text to the Fig. 6 caption to guide the reader to this information: "Detailed statistics of the "truth", multi-model means of prior and posterior NEE estimates, standard deviations, and ranges displayed in this figure are listed in Table 3.". In response to the reviewer, we have added Table S1 and S2 to the supplementary material of the revised manuscript in order to provide the "truth", mean, standard deviation, and range of the NEE values calculated in the sensitivity studies of prior error statistics and ocean glint (OG) simulations, respectively (detailing Fig 7 and 8).

2. My main complaint with this is that there are a few papers out there now that use ensembles of models for inference (Basu et al, 2018; Crowell et al, 2019; older ones like Peylin et al, 2013), and that this would be a much more effective paper if it were to place itself in the context of the "uncertainty budget" for these other papers. For example, Crowell et al (2019) presents results in the form of ensemble means and standard deviations, and Basau et al (2018) presents ensemble members individually, and the results here could be placed beside the Basu et al (2018) results to attempt to explain the scatter in the flux results in Crowell et al (2019). That sort of analysis would elevate the messages in this paper to a greater impact.

We fully agree with the reviewer that the comparison of our results with Crowell et al. (2019) and Basu et al. (2018) is important and will greatly improve the impact of this study. We thought of this prior to submission of our manuscript, however, Crowell et al. (2019) (along with the OCO-2 Multi-model Inter-comparison Project (MIP) Level 4 (L4) CO_2 flux data) and the supplementary tables of Basu et al. (2018) were not yet published. However, now that this information is available, we have performed the suggested comparison and have added the following text to the conclusions section of the revised manuscript:

"As explained earlier in this study, estimates of surface CO_2 fluxes from numerous inversion systems in the OCO-2 MIP ensemble model framework, using identical OCO-2 observations, result in different optimized/posterior regional NEE fluxes (Crowell et al., 2019). This inverse model variance can be due to numerous factors (e.g., model transport, inversion methods, observation errors, etc.) including prior model mean and uncertainty estimates. In order to estimate the amount of variance in the results of posterior NEE values from the OCO-2 MIP which could be due to prior flux estimates, we compare our OSSE derived residual posterior NEE range (using LN+LG) to the range in the posterior Level-4 OCO-2 Flux data (using both LN and LG) (https://www.esrl.noaa.gov/gmd/ccgg/OCO2/index.php) in each TransCom-3 region. This comparison suggests that prior NEE and uncertainty statistics could contribute 10-30% (average ~20%) of annually-averaged NEE variance calculated for each TransCom-3 region in the OCO-2 Level-4 MIP flux data. Comparing this contribution of prior model impact to the OSSE study by Basu et al. (2018), which calculated the impact of atmospheric transport on posterior NEE estimates when assimilating OCO-2 observations, this contribution is ~50% less compared to the impact of atmospheric transport. From our study and Basu et al. (2018) it is estimated that the combination of prior flux/uncertainty assumptions and atmospheric transport could contribute on average ~50% of the annually-averaged posterior NEE variance of the OCO-2 MIP study."

Also, the references to "Crowell et al. in prep." have been updated to "Crowell et al., 2019".

Specific comments: Page 4, Line 28 - how much do the models really vary using this approach? I'd guess not much. Can you provide a figure at a well known flux tower site as a demonstration?

A similar comment was made by the editor on behalf of an additional referee. In order to demonstrate the difference between the "true" NEE and prior model data in regards to diurnal variability, monthly-averaged 3-hourly (MsTMIP) and hourly (for the 4 prior biosphere models) NEE values were plotted for July 2015 at the well-known Park Falls flux tower site (45.95°N, 90.27°W). This figure has been added to the revised manuscript in the supplementary section as Fig. S1. We added additional text to Sect. 2.1 of the revised manuscript which reads: "We allow the "true" and prior models to have different diurnal variability in order to represent a realistic scenario, as prior models will differ some from the actual diurnal variability of NEE in nature. In general, the diurnal variability of NEE is similar between the "true" and individual prior models. An example is shown in Fig. S1 where it can be seen that the diurnal NEE from the "true" and prior models for July 2015 at the Park Falls flux tower site (45.95°N, 90.27°W) have near identical temporal diurnal patterns and only differ in NEE magnitude.".

Page 7, Line 16-18 Chevallier et al also went after this by looking at structural uncertainties in the ORCHIDEE ecosystem model. Chevallier, F., Viovy, N., Reichstein, M., & Ciais, P. (2006). On the assignment of prior errors in Bayesian inversions of CO_2 surface fluxes. Geophysical Research Letters, 33(13), L13802. https://doi.org/10.1029/2006GL026496

We appreciate the reviewer pointing out this study. We have added this reference to the revised manuscript and additional text in Sect. 2.4.5 which reads: "…, using continuous in situ measurements of CO_2 flux compared to model simulations to inform prior errors (Chevallier et al., 2006), …"

Page 8, Lines 5-9 - these errors are even smaller than those predicted by the Level 2 retrieval, and those are known to be underestimated (from various uncertainty quantification talks). I wonder, could this really be a sign that your prior errors need tuning, rather than your observation errors? In the OSSE setting, it's equivalent which way you go, but in real data settings, this choice can matter a lot. There are other metrics to optimize the prior errors vs. the observational error statistics, such as the Desrozier approach (commonly used in numerical weather prediction)

We agree with the reviewer that the observational error values applied to our OSSE simulations for synthetic OCO-2 data are smaller than that in the real data. It should be noted that the simulated synthetic OCO-2 data produced in this study is done so using known fluxes and transport and sampling a model-predicted atmosphere, thus errors should be small. This manner of producing synthetic satellite observations makes it so there is no model-data mismatch or systematic error which is the major fraction of OCO-2 error values.

The reviewer is correct in the fact that the manner in which observational and prior error are adjusted is equivalent for OSSE simulations (such as this work), however, can impact the results of posterior estimates in "real" inverse model simulations. In addition to the fact we use model produced observations in our OSSEs, we also decided not to reduce our prior error statistics in order to be representative of how prior error is typically calculated/treated in "real" data assimilations. Calculating the difference or spread between state-of-the-science model ensemble members as the best estimate of our knowledge of a process is commonly done to define prior error values. Furthermore, if prior error values are reduced and observation error remain large, this results in an inversion system which is limited in the ability to deviate from the prior and posterior NEE spread calculated would be due to both observational error and prior NEE flux/error. Therefore, by reducing observational error (attached to data which have no model-data mismatch or systematic error in our OSSE framework), and defining prior error as is done in "real" inversions, provides a true representation of the spread in posterior estimates primarily due to prior flux/error.

Page 10, Lines 34-35 - this is often called the "uncertainty reduction", assuming the standard deviation is a proxy for the uncertainty.

We have modified the following text in Sect. 3.4 of the revised manuscript to demonstrate this: "The reduction in the SD of NEE (also known as uncertainty reduction) in most regions/seasons, calculated as 100 × (1 – (posterior NEE SD)/(prior NEE SD)) is generally > 70% and up to 98%".

References

Basu, S., Baker, D. F., Chevallier, F., Patra, P. K., Liu, J., and Miller, J. B.: The impact of transport model differences on CO_2 surface flux estimates from OCO-2 retrievals of column average CO_2, Atmos. Chem. Phys., 18, 7189-7215, https://doi.org/10.5194/acp-18-7189-2018, 2018.

Chevallier, F., Viovy, N., Reichstein, M., and Ciais, P.: On the assignment of prior errors in Bayesian inversions of CO_2 surface fluxes, Geophys. Res. Lett., 33, L13802, https://doi.org/:10.1029/2006GL026496, 2006.

Crowell, S., Baker, D., Schuh, A., Basu, S., Jacobson, A. R., Chevallier, F., Liu, J., Deng, F., Feng, L., McKain, K., Chatterjee, A., Miller, J. B., Stephens, B. B., Eldering, A., Crisp, D., Schimel, D., Nassar, R., O'Dell, C. W., Oda, T., Sweeney, C., Palmer, P. I., and Jones, D. B. A.: The 2015–2016 carbon cycle as seen from OCO-2 and the global in situ network, Atmos. Chem. Phys., 19, 9797–9831, https://doi.org/10.5194/acp-19-9797-2019, 2019.

Response to Anonymous Referee (through Editor's comments)

We thank the editor for adding these addition valuable reviewer comments. Throughout the document reviewer comments are displayed in standard font while author responses are presented with blue text.

The investigators have conducted a series of OSSEs to assess the impact of prior biospheric fluxes on posterior fluxes in CO_2 flux inversions using OCO-2 data. The lack of robust regional flux estimates is a major issue in the flux inversion community. It is known that the choice of prior fluxes can impact posterior flux estimates, contributing to discrepancies between different inversions. This study has conducted the most detailed and thorough sensitivity analysis to date to quantify the potential impact of the prior fluxes in CO_2 inversions. The manuscript is well written and I recommend it for publication in ACP with minor revisions to address my mostly technical comments below.

Comments

1. Page 4, line 3-4: Change "NEE flux (balanced biosphere)" to just "NEE flux".

We have removed the following text "(balanced biosphere for the 1998-2017 time period)" in the revised manuscript.

2. Page 4, line 28: How different is the diurnal variation between the truth and the prior models? This information could be included in the Supplement.

A similar comment was made by Referee #4. In order to demonstrate the difference between the "true" NEE and prior model data in regards to diurnal variability, monthly-averaged 3-hourly (MsTMIP) and hourly (for the 4 prior biosphere models) NEE values were plotted for July 2015 at the well-known Park Falls flux tower site (45.95°N, 90.27°W). This figure has been added to the revised manuscript in the supplementary section as Fig. S1. We added additional text to Sect. 2.1 of the revised manuscript which reads: "We allow the "true" and prior models to have different diurnal variability in order to represent a realistic scenario, as prior models will differ some from the actual diurnal variability of NEE in nature. In general, the diurnal variability of NEE is similar between the "true" and individual prior models. An example is shown in Fig. S1 where it can be seen that the diurnal NEE from the "true" and prior models for July 2015 at the Park Falls flux tower site (45.95°N, 90.27°W) have near identical temporal diurnal patterns and only differ in NEE magnitude.".

3. Page 6, line 2: Change "CO_2 at August" to "CO_2 on August".

This has been corrected.

4. Page 6, line 13: OCO-2 XCO2 is not actually retrieved using Equation (1). Rather, the retrieval is expressed as Equation (1), after the fact.

The following text "OCO-2 XCO2 is retrieved using the following equation" has been changed to "The retrieval of OCO-2 XCO2 is expressed as Eq. (1)" in the revised manuscript.

5. Page 6, line 16: Please add "column" between "a" and "averaging" kernel.

This has been corrected.

6. Page 6, lines 32, 34, 35, etc...: Please change "model grid" to "model grid box" when discussing the model grid boxes. For example, on lines 34-35 it should read "the j^{th} model grid box" instead of the "j^{th} model grid".

This has been corrected.

7. Page 7, line 5, and page 8, line 31: Same comment as above regarding the "model grid" vs "model grid box".

This has been corrected

8. Page 7, Equation (3): Shouldn't this equation be similar to Equation (1) since the observation operator is transforming the model into the observation space? For example, the "ya" and "Ma" in this equation should be the same as "ca" and "XCO2a" used in Equation (1), respectively. The only quantity that should be different in this expression is "f(x)", which represents the simulated profile.

We thank the reviewer for recognizing this. In the updated manuscript we now use the same symbols for the prior CO_2 profile and column CO_2 values from OCO-2 data in the retrieval (Eq. (1)) and observation operator (Eq. (3)) description.

9. Page 7, line 37: Something is missing between "Similar" and "to prior error statistics". Should this say "Similar to our treatment of the prior error statistics:"

This text in the revised manuscript has been corrected to "Similar to the treatment of prior error statistics".

10. Page 8, lines 20: Figure S2 is useful for the reader who is unfamiliar with the TransCom domains. Furthermore, it has the numerical ordering of the regions that is useful for interpreting Table 3. I would suggest moving this into the main manuscript.

We thank the reviewer for this suggestion and we have moved this figure from the supplementary material to be Fig. 1 in the main manuscript.

11. Page 10: Figures S5 and S7 show the spatial distribution of the results and complements the information shown in Figures 3-5. I would suggest moving Figures S5 and S7 in the main section of the manuscript, which currently has only five figures.

We thank the reviewer for this suggestion and we have moved Fig. S5 and S7 from the supplementary material to the main manuscript and are now Fig. 3 and 5, respectively.

12. Page 11, lines 31-33: I don't understand the statement here that the NEE estimates are more sensitive to the prior error when there are sufficient observations available and large differences between the truth and prior. Is this due to the inversion approach used here? Is it because the prior error is a relative error so when the flux is larger, the error is also larger, which gives the inversion more flexibility in adjusting the fluxes?

We refer the reviewer to the end of Sect. 2.4.5 where the discussion of the prior error calculations is presented. In this study, we calculate prior error values from the standard deviation (SD) of the four prior models (as a NEE magnitude) which is then divided by the magnitude of the NEE flux from each individual model (fractional error). We did this in order for our relative error values (fractional error) to be representative of absolute error magnitudes as defined by the SD calculation. This is done so large prior error can be applied to small fluxes and vice versa.

The reason that posterior NEE estimates are more sensitivity to prior error values in regions with sufficient observational coverage/density and large differences in "true" and prior fluxes is as follows. When the model

has sufficient observations to constrain NEE fluxes, and the "truth" and prior are noticeably different, the model must optimize the prior flux significantly to match the truth. When the prior error is too small (e.g., 10% in all grid boxes as we apply in our sensitivity study), the model will not have enough freedom to deviate from the prior estimate to match the truth. For cases when large prior error is assigned (e.g., 100% in all grid boxes), the model is able to diverge greatly from the prior in all regions in order to match observations. As demonstrated in Sect. 3.3 of the manuscript, when applying different prior NEE estimates, the model will optimize CO_2 fluxes in variable ways to match atmospheric observations. The larger the prior error applied to each prior flux will add additional flexibility in each simulation allowing the model to match the atmospheric observations in increasingly different ways when using variable prior fluxes.

Prior biosphere model impact on global terrestrial CO_2 fluxes estimated from OCO-2 retrievals

Sajeev Philip[1,2,*], Matthew S. Johnson[1], Christopher Potter[1], Vanessa Genovesse[3,1], David F. Baker[4,5], Katherine D. Haynes[6], Daven K. Henze[7], Junjie Liu[8], and Benjamin Poulter[9]

[1]NASA Ames Research Center, Moffett Field, CA 94035, USA
[2]NASA Postdoctoral Program administered by Universities Space Research Association, Columbia, MD 21046, USA
[3]California State University, Monterey Bay, CA 93955, USA
[4]NOAA Earth System Research Laboratory, Global Monitoring Division, Boulder, CO 80305-3337, USA
[5]Cooperative Institute for Research in the Atmosphere, Colorado State University, Ft. Collins, CO 80521, USA
[6]Department of Atmospheric Science, Colorado State University, Fort Collins, CO 80523, USA
[7]Department of Mechanical Engineering, University of Colorado at Boulder, Boulder, CO 80309, USA
[8]Jet Propulsion Laboratory, California Institute of Technology, Pasadena, CA 91109, USA
[9]NASA Goddard Space Flight Center, Greenbelt, MD 20771, USA
[*]Now at NASA Academic Mission Services by Universities Space Research Association, Mountain View, CA 94043, USA

Correspondence to: Sajeev Philip (philip.sajeev@gmail.com) and Matthew S. Johnson (matthew.s.johnson@nasa.gov)

Abstract. This study assesses the impact of different state-of-the-science global biospheric CO_2 flux models, when applied as prior information, on inverse model "top-down" estimates of terrestrial CO_2 fluxes obtained when assimilating Orbiting Carbon Observatory 2 (OCO-2) observations. This is done with a series of Observing System Simulation Experiments (OSSEs) using synthetic CO_2 column-average dry air mole fraction (XCO_2) retrievals sampled at the OCO-2 satellite spatio-temporal frequency. The OSSEs used a four-dimensional variational (4D-Var) assimilation system with the GEOS-Chem global chemical transport model (CTM) to estimate CO_2 net ecosystem exchange (NEE) fluxes using synthetic OCO-2 observations. The impact of biosphere models in inverse model estimates of NEE is quantified by conducting OSSEs using the NASA-CASA, CASA-GFED, SiB-4 and LPJ models as prior estimates and using NEE from the multi-model ensemble mean of the Multiscale Synthesis and Terrestrial Model Intercomparison Project as the "truth". Results show that the assimilation of simulated XCO_2 retrievals at OCO-2 observing modes over land results in posterior NEE estimates which generally reproduce "true" NEE globally and over terrestrial TransCom-3 regions that are well-sampled. However, we find larger spread among posterior NEE estimates, when using different prior NEE fluxes, in regions and seasons that have limited OCO-2 observational coverage and a large range in "bottom-up" NEE fluxes. Seasonally-averaged posterior NEE estimates had standard deviations (SD) of ~10% to ~50% of the multi-model-mean NEE for different TransCom-3 land regions with significant NEE fluxes (regions/seasons with a NEE flux $\geq$ 0.5 PgC yr^{-1}). On a global average, the seasonally-averaged residual impact of the prior model NEE assumption on posterior NEE spread is ~10-20% of the posterior NEE mean. Additional OCO-2 OSSE simulations demonstrate that posterior NEE estimates are also sensitive to the assumed prior NEE flux uncertainty statistics, with spread in posterior NEE estimates similar to those when using variable prior model NEE fluxes. In fact, the sensitivity of posterior NEE estimates to prior error statistics was larger compared to prior flux values in some regions/times in the Tropics and Southern Hemisphere where sufficient OCO-2 data was available and large differences between the prior and "truth" were evident. Overall, even with the availability of spatio-temporally dense OCO-2 data, noticeable residual differences (up to ~20-30% globally and 50% regionally) in posterior NEE flux estimates remain that were caused by the choice of prior model flux values and the specification of prior flux uncertainties.

Deleted: ing

Deleted: the

Deleted: P

Deleted: seasonally-averaged posterior NEE

Deleted: of

1 Introduction

Carbon dioxide (CO_2) is the most important greenhouse gas (GHG) contributing to climate change on a global scale (IPCC, 2014). The anthropogenic emission of CO_2, primarily from fossil fuel usage, has led to average global CO_2 mixing ratios reaching historically high levels of > 400 parts per million (ppm) (Seinfeld and Pandis, 2016). In addition to fossil fuel emissions, the processes involved in the exchange of carbon between the atmosphere and terrestrial biosphere are a major factor controlling atmospheric concentrations of CO_2 (e.g., Schimel et al., 2001) with an estimated global biosphere sink of ~3.0 PgC yr^{-1} (Le Quéré et al., 2018). However, current estimates of regional-scale atmosphere-terrestrial biosphere CO_2 exchange have large uncertainties (Schimel et al., 2015). "Bottom-up" techniques typically simulate the atmosphere-terrestrial biosphere exchange based on our understanding of these complex exchange processes and by constraining these estimates with remote-sensing inputs and limited measurements available for evaluation. Previous studies inter-comparing several of the most commonly used biospheric flux models (Heimann et al., 1998, Huntzinger et al., 2012; Sitch et al., 2015; Ott et al., 2015; Ito et al., 2016) and multi-model ensemble integration projects (Schwalm et al., 2015) reveal a large spread among global/regional "bottom-up" terrestrial biospheric flux estimates and the sub-components such as ecosystem primary production and respiration (Huntzinger et al., 2012).

An alternate approach to estimate biospheric CO_2 fluxes is through "top-down" estimation techniques using inverse models with highly accurate in situ data (e.g., Baker et al., 2006b) or dense and globally distributed satellite data (e.g., Chevallier et al., 2005). The Orbiting Carbon Observatory-2 (OCO-2) satellite, launched in 2014, is the space-borne sensor with the finest resolution and highest sensitivity of CO_2 in the atmospheric boundary layer to date (Crisp et al., 2017; Eldering et al., 2017a). Studies applying OCO-2 retrievals revealed the ability to investigate novel aspects of the carbon cycle (e.g., Eldering et al., 2017b; Liu et al., 2017), however, the "top-down" estimates of surface CO_2 fluxes from numerous inverse modeling systems, using identical OCO-2 observations, show differences among optimized/posterior regional CO_2 fluxes (Crowell et al., 2019). Previous studies investigating CO_2 flux inversions (e.g., Peylin et al., 2013; Chevallier et al., 2014; Houweling et al., 2015) suggest that this spread among optimized CO_2 flux estimates could be due to numerous factors, such as the accuracy and precision of observation data (Rödenbeck et al., 2006), imperfect observation coverage (Liu et al., 2014; Byrne et al., 2017), data density (Law et al., 2003; Rödenbeck et al., 2003) and poorly characterized measurement error covariance (Law et al., 2003; Takagi et al., 2014). Variations in inverse estimation setups between modeling groups, such as model transport (Chevallier et al., 2010; Houweling et al., 2010; Basu et al., 2018) and inversion methods (Chevallier et al., 2014; Houweling et al., 2015), could also lead to inter-model spread in posterior estimates.

In addition to the variables listed above, the assumed prior fluxes and the associated prior error covariance can also impact "top-down" global/regional CO_2 flux estimates (e.g., Gurney et al., 2003). Gurney et al. (2003) assessed the sensitivity of CO_2 flux inversions to the specification of prior flux uncertainty and found that the posterior estimates were sensitive to the prior fluxes over regions with limited in situ observations. In addition, Wang et al. (2018) found that optimal CO_2 flux allocation over land versus ocean, using satellite and/or in situ data assimilations, is sensitive to the specification of prior flux uncertainty. Furthermore, Chevalier et al. (2005) and Baker et al. (2006a; 2010) highlighted the importance of accurate assumptions of prior flux uncertainty by conducting four-dimensional variational (4D-Var) assimilations of satellite column retrievals of CO_2. However, to date, there are no controlled experimental studies to isolate and quantitatively assess the impact of assumed prior fluxes and prior uncertainty to inverse estimates of biospheric CO_2 fluxes using satellite observations.

Therefore, during this study we conduct a series of controlled experiments to quantitatively assess the impact of assumed prior fluxes and prior uncertainty on global and regional CO_2 inverse model flux estimates when assimilating OCO-2 data. In order to achieve this, a series of Observing System Simulation Experiments (OSSEs) are conducted using synthetic OCO-2 observations in the GEOS-Chem 4D-Var assimilation system, with four different prior "bottom-up" NEE CO_2 flux estimates. Section 2 of this

Deleted: -

Deleted: in prep

study describes the methods applied during this work including individual models and model input, synthetic OCO-2 data and the inversion technique applied in the OSSEs. Section 3 presents the forward and inverse model results of simulated atmospheric CO_2 concentrations and inferred posterior flux estimates. Finally, our concluding remarks and discussion are presented in Section 4.

Deleted: described

2 Methods

To quantify the impact of prior model NEE predictions on posterior estimates of biospheric CO_2 fluxes, a series of CO_2 forward and inverse model simulations were conducted with four different state-of-the-science biosphere models. OSSE simulations were designed to isolate the differences in posterior NEE estimates caused by the selection of prior model biospheric CO_2 fluxes and uncertainties when assimilating OCO-2 observations. The OSSE framework, input variables, inversion technique and analysis method are presented below.

2.1 Prior NEE fluxes

NEE is the net difference of gross primary production (GPP) and total ecosystem respiration (R_e), which itself is the sum of autotrophic respiration (R_a) and heterotrophic respiration (R_h). NEE, estimated by terrestrial biospheric CO_2 flux models, is commonly applied in CTMs to simulate atmosphere-terrestrial biosphere carbon exchange. Many biosphere carbon models estimate GPP and R_e, however, some models simulate net primary productivity (NPP), which is defined as the difference between GPP and R_a. In this study, we apply year-specific NEE fluxes calculated from four state-of-the-science biosphere models: 1) NASA Carnegie Ames Stanford Approach (NASA-CASA), 2) CASA-Global Fire Emissions Database (CASA-GFED), 3) Simple-Biosphere model version 4 (SiB-4) and 4) Lund-Potsdam-Jena (LPJ). It should be noted that the prior biosphere models used in this study include only NEE and a single dataset for wild fire and fuel wood burning CO_2 emissions was added separately (see Sect. 2.3). The models applied during this study represent a range of diagnostic approaches, from models predicting biospheric CO_2 fluxes using remotely-sensed data (e.g., Fraction of Absorbed Photosynthetically Active Radiation, Leaf Area Index, Normalized Difference Vegetation Index) to fully prognostic models unconstrained by observations. In addition, we selected both balanced/neutral (SiB-4) and non-balanced (NASA-CASA, CASA-GFED, LPJ) biospheric fluxes in our OSSEs in order to represent the range of prior models currently being used in CO_2 inversion modeling studies.

CASA is an ecosystem model predicting NPP based on light use efficiency and R_h based on soils/plant production information (Potter et al., 1993; 2012b). The NASA-CASA model is a version of the original CASA model (Potter et al., 1993) currently being developed at NASA Ames Research Center (Potter et al., 2003; 2007; 2009; 2012a; 2012b). NASA-CASA specifically utilizes data on global vegetation cover (Enhanced Vegetation Index, Surface Solar Irradiance Data) and land disturbances retrieved from the NASA Moderate Resolution Imaging Spectroradiometer (MODIS) satellite (Potter et al., 2012b). In addition to R_h, NASA-CASA includes redistributed crop harvest CO_2 emissions to the atmosphere (Potter et al., 2012b). The CASA-GFED model is a different version of the original CASA model and is described in Randerson et al. (1996) with subsequent versions being described in recent literature (van der Werf et al., 2004; 2006; 2010). NASA-CASA and CASA-GFED differ in the use of input parameters and some of the parameterizations (see Ott et al. (2015) for further description).

Deleted: enhanced
Deleted: vegetation
Deleted: index
Deleted: surface
Deleted: solar
Deleted: irradiance
Deleted: data

The SiB-4 model was developed at Colorado State University (Sellers et al., 1986; Denning et al., 1996) with details of the newest versions described in Haynes et al. (2013). This model is a mechanistic, prognostic land surface model that integrates heterogeneous land cover, environmentally responsive prognostic phenology, dynamic carbon allocation and cascading carbon pools from live biomass to surface litter and soil organic matter (Haynes et al., 2013; Baker et al., 2013; Lokupitiya et al., 2009; Schaefer et al., 2008; Sellers et al., 1996). By combining biogeochemical, biophysical and phenological processes, SiB-4 predicts vegetation and soil moisture states, land surface energy and water budgets and the terrestrial carbon cycle. Rather than relying on

satellite input data, SiB-4 fully simulates the terrestrial carbon cycle by using the carbon fluxes to determine the above and below-ground biomass, which in turn feed back to impact carbon assimilation and respiration. Similar to NASA-CASA, the SiB4 model redistributes crop harvest CO_2 emission to the atmosphere. Note that we use a balanced (neutral) biospheric NEE flux for the SiB-4 model.

The LPJ model is a process-based dynamic global vegetation model (Sitch et al., 2003; Polter et al., 2014). The LPJ-wsl dynamic global vegetation model (Sitch et al., 2003) was used to simulate NEE using meteorological data from the Climate Research Unit (Harris et al., 2013). LPJ is fully prognostic, meaning that the establishment, growth and mortality of vegetation are represented by first-order physiological principles. The model includes nine plant functional types distinguished by their phenology, photosynthetic pathway and physiognomy. Phenology status is determined daily and photosynthesis is estimated using a modified Farquhar scheme (Haxeltine and Prentice, 1996). NPP is calculated from photosynthesis after accounting for R_a and reproductive allocation. The LPJ-wsl model has been evaluated in several benchmarking activities for stocks and fluxes (Peng et al., 2015; Sitch et al., 2015).

In order to provide a "true" NEE flux for the OSSEs conducted in this study (Sect. 2.4), we use the multi-model ensemble NEE mean from the Multiscale Synthesis and Terrestrial Model Intercomparison Project (MsTMIP) (Huntzinger et al., 2013; 2018; Fisher et al., 2016a; 2016b). The MsTMIP NEE fluxes are from a weighted ensemble mean of 15 biosphere models (Schwalm et al., 2015) for the year 2010. Here we apply the MsTMIP data for year 2010 as the "truth" with year-specific prior model predictions for 2015. This procedure is justified in our case as within an OSSE framework there needs to be a difference between "true" and prior fluxes, as long as the "true" values are realistic in nature. The MsTMIP ensemble NEE mean represents a summary over all 15 models which smooths out errors particular to any given model. This "true" NEE flux is used to produce the synthetic OCO-2 observations applied in this study (described further in Sect. 2.4.3).

The "true" and four prior model NEE fluxes were regridded from their native horizontal resolutions to the grid resolution of the inverse model simulations (4.0° latitude × 5.0° longitude). The MsTMIP NEE fluxes are provided as 3-hourly averages and the four year-specific prior models were provided as monthly-mean GPP or NPP and R_e or R_h. Therefore, we imposed diurnal (hourly) and daily variability to these four prior models following the approach in CarbonTracker CT2016 (http://carbontracker.noaa.gov), which is based on Olsen and Randerson (2004). This hourly/daily NEE variability for each prior model was calculated using the downward solar radiation flux and 2-meter air temperature data from the GEOS-FP (Goddard Earth Observing System Model, Version 5 "Forward Processing") meteorological product and monthly-averaged GPP and R_h from the respective model. We allow the "true" and prior models to have different diurnal variability in order to represent a realistic scenario, as prior models will differ some from the actual diurnal variability of NEE in nature. In general, the diurnal variability of NEE is similar between the "true" and individual prior models. An example is shown in Fig. S1 where it can be seen that the diurnal NEE from the "true" and prior models for July 2015 at the Park Falls flux tower site (45.95°N, 90.27°W) have near identical temporal diurnal patterns and only differ in NEE magnitude. Table 1 shows the global annual NEE flux estimates for the four prior models and the "truth". From this table it can be seen that the MsTMIP product shows a strong annual global sink of -4.31 PgC yr^{-1}. NASA-CASA and CASA-GFED predict a global sink of ~2 PgC yr^{-1} and differ by ~0.6 PgC yr^{-1}. SiB-4 NEE predicts a source of ~1 PgC yr^{-1} and the LPJ model predicts a strong sink of ~5.5 PgC yr^{-1}. Section 3.1 further describes the spatio-temporal differences of the NEE fluxes between these four prior models and the "truth".

2.2 GEOS-Chem model

The GEOS-Chem chemical transport model (CTM) (http://geos-chem.org; Bey et al., 2001) used in this study has the capability to run forward CO_2 simulations (Suntharalingam et al., 2004; Nassar et al., 2010) and corresponding adjoint model calculations

Deleted: (balanced biosphere for the 1998-2017 time period)

Deleted: and the

Deleted: "true"

Deleted: We allow the "true" and prior models to have different diurnal variability in order to represent a realistic scenario, as prior models will differ some from the actual diurnal variability of NEE in nature. In general, the diurnal variability of NEE is similar between the "true" and individual prior models. An example is shown in Fig. S1 where it can be seen that the diurnal NEE from the "true" and prior models are similar for July 2015 at the Park Falls flux tower site (45.95°N, 90.27°W) having very little temporal variance and only differences in NEE magnitude.

(Henze et al., 2007; Liu et al., 2014). In this study, we use the GEOS-Chem adjoint version 35, which is compatible with version 8-02 of the GEOS-Chem forward model. Liu et al. (2014) tested the accuracy of the GEOS-Chem CO_2 adjoint system, which has been used for several CO_2 inverse modeling studies (e.g., Liu et al., 2017; Bowman et al., 2017; Deng et al., 2014). The model is driven with assimilated meteorological fields from the GEOS-FP model of the NASA Global Modeling Assimilation Office (GMAO). The GEOS-FP meteorology fields have a native horizontal resolution of 0.25° × 0.3125° and 72 native hybrid sigma-pressure vertical levels from the Earth's surface to 0.01 hPa. We conduct simulations with a coarser spatial resolution (4.0° × 5.0°) with 47 reduced vertical levels to attain reasonable computational efficiency.

2.3 Non-NEE CO_2 fluxes

To simulate concentrations of atmospheric CO_2, we used several land and ocean CO_2 flux inventories in addition to the NEE estimates from the prior biosphere models (global annual budgets listed in Table 1). This study used the year-specific fossil fuel and cement production inventory from the Open-source Data Inventory for Anthropogenic CO_2 (ODIAC-2016) developed by Oda et al. (2018). Following the approach of Nassar et al. (2013), the monthly ODIAC-2016 inventory is converted from the native temporal variability into diurnal (hourly) and weekday/weekend variability (courtesy: Sourish Basu and the OCO-2 Science Team). Wild fire emissions and fuel wood burning emissions were taken from the 3-hourly Global Fire Emissions Database (GFED3) database. Shipping emissions are from the International Comprehensive Ocean-Atmosphere Data Set (ICOADS) (Corbett and Koehler, 2003; 2004) and aviation emissions are from the Aviation Emissions Inventory Code (AEIC) inventory (Olsen et al., 2013). We used 3D chemical production of CO_2 from the oxidation of carbon monoxide, methane and non-methane volatile organic compounds (Nassar et al., 2010). The shipping, aviation and 3D chemical source are climatological and are taken from the Bowman (2017) dataset. To simulate oceanic CO_2 fluxes, we apply the year-specific 3-hourly posterior estimates from the CarbonTracker 2016 (CT2016) model constrained with in situ data (Peters et al., 2007; http://carbontracker.noaa.gov). All emission inventories, besides NEE fluxes, are kept constant between the different inverse model simulations.

Deleted: varying

2.4 Observing System Simulation Experiments (OSSEs)

2.4.1 OSSE framework

This study conducted several OSSEs to assess the impact of prior biospheric CO_2 models and associated prior uncertainty specifications on posterior estimates of NEE when assimilating OCO-2 data. To assess the impact of prior fluxes, we conduct four baseline OSSEs (using the four prior biosphere models) assimilating synthetic land nadir (LN) and land glint (LG) observations together, plus an additional four OSSEs using just ocean glint (OG) observations. These OSSE simulations were designed in such a way that the differences in posterior NEE estimates are due solely to the choice of prior biospheric flux (e.g., identical initial atmospheric CO_2 conditions, non-NEE fluxes, OCO-2 sampling frequency, observational data uncertainty, etc.). Furthermore, to assess the impact of prior uncertainty specifications, we conduct two additional OSSEs (in addition to our baseline prior uncertainty assumption described in Sect. 2.4.5) with synthetic LN and LG observations using prior error set uniformly to 10% and 100% of a particular prior NEE flux (CASA-GFED). Table 2 shows the summary of OSSEs conducted for this study. During all OSSE simulations NEE and oceanic CO_2 fluxes are optimized, with all other sources kept constant, in order to be consistent with the methods commonly used by inverse modeling systems focused on estimating NEE. We optimize oceanic fluxes together with NEE, although the same ocean fluxes were used for the "truth" and the prior in all OSSE simulations (Sect. 2.3) for simplicity and because the terrestrial NEE fluxes are the focus of this work. It is noteworthy that the assimilation of land or ocean data in fact do not produce substantial deviations from the "truth" over the TransCom-3 oceanic regions (Fig. S2). For all OSSE simulations, an assimilation window of 18 months covering the period from August 1, 2014 to January 31, 2016 was applied. NEE/oceanic fluxes

Deleted: S1

are optimized for every month of the assimilation window at each surface grid box in the GEOS-Chem model. The analysis of prior and posterior NEE fluxes is for all months in 2015, treating the other months as spin-up and spin-down periods.

2.4.2 Initial CO_2 concentrations

We use identical initial atmospheric concentrations of CO_2 on August 1, 2014 for: 1) the GEOS-Chem forward model simulations generating synthetic XCO_2 using the "true" NEE fluxes (Sect. 2.4.3) and 2) for all the OSSEs using variable prior biosphere model predictions. The initial CO_2 concentrations were generated by running the GEOS-Chem forward model for two years using the "true" MsTMIP NEE and other non-NEE CO_2 sources. The restart file used for this two year forward model run was taken from an earlier GEOS-Chem model simulation constrained with in situ observations (personal communication from Ray Nassar) in order to represent a realistic initial condition.

2.4.3 Synthetic OCO-2 retrievals

In this study, we used synthetic satellite data that is directly representative of version 8 of the OCO-2 product. The OCO-2 satellite sensor is in sun-synchronous polar orbit with a repeat cycle of 16 days and a local over-pass time in the early afternoon (Crisp et al., 2017). OCO-2 has three different viewing modes: soundings over land from LN and LG and over oceans from OG. The algorithm of O'Dell et al. (2012) is used to retrieve column-average dry air mole fraction of CO_2 (XCO_2) and other retrieval variables. The retrieval of OCO-2 XCO_2 is expressed as Eq. (1), using a prior CO_2 vertical profile ($\mathbf{c}_a$) and prior CO_2 column ($XCO_{2\,(a)}$) value,

$$XCO_2 = XCO_{2\,(a)} + \mathbf{a}^{\mathrm{T}}(\mathbf{c} - \mathbf{c}_a) \qquad (1)$$

where $\mathbf{c}$ is the true profile of CO_2 concentrations and $\mathbf{a}$ is the column averaging kernel. The individual soundings of OCO-2 are at a fine-resolution (24 spectra per second with < 3 km^2 spatial resolution per sounding), leading to a very large data volume (Crisp et al., 2017). This level of detail is lost when the measurements are used in global inverse models with much coarser spatial resolution, with numerous individual OCO-2 soundings occur in a single model grid box. In addition, each sounding does not really provide an independent piece of information to the inversion system due to spatial and temporal error correlations. Therefore, we use 10-sec averages of the individual XCO_2 soundings similar to those developed/described in Basu et al. (2018), however, from an updated version with file name: OCO2_b80_10sec_WL04_GOOD_v2.nc. This 10-sec data contains averages of retrievals with a "GOOD" quality flag and Warn Level from 1 to 4. Note that in this study we do not use actual retrieved 10-sec XCO_2 values for our OSSEs, however, synthetic XCO_2 data were generated corresponding to the spatio-temporal sampling frequency of version 8 OCO-2 10-sec data. The synthetic 10-sec XCO_2 data is calculated with the CO_2 concentration profile simulated using the GEOS-Chem forward model (using MsTMIP as the NEE flux model). In this manner we produced synthetic XCO_2 data that is representative of the "true" atmosphere corresponding to the "true" NEE fluxes used in this study. We archived these synthetic XCO_2 data and applied them for all OSSEs conducted.

2.4.4 Inverse modeling approach

The transport of atmospheric CO_2 is simulated using GEOS-Chem along with prescribed surface fluxes as input data (see Table 1). Subsequently, the GEOS-Chem 4D-Var inverse modeling system assimilates synthetic OCO-2 XCO_2 data to estimate the posterior/optimized monthly-mean NEE and oceanic fluxes at each surface grid box of the model. The GEOS-Chem adjoint system applies the L-BFGS numerical optimization algorithm with a no-bound option (Liu and Nocedal, 1989). Posterior monthly-averaged NEE/oceanic fluxes ($\mathbf{x}$) are inferred for each surface model grid box by optimizing a vector of scaling factors σ_j for the j^{th} model grid box,

Deleted: at

Deleted: OCO-2 XCO_2 is retrieved using the following equation

Deleted: ,

Deleted: vector

Deleted: cell

$$x_j = \sigma_j \, x_{a,j} \quad (2)$$

where $\mathbf{x}_a$ represents the monthly-mean prior NEE/oceanic fluxes. Scaling factors are assumed to be unity at the first iteration (that is, prior NEE flux itself is used). The inversion system, as described below, optimizes the scaling factor applied to the monthly-mean fluxes and the posterior scaling factors are then used to scale prior fluxes to infer posterior CO_2 fluxes.

For each iteration, the inversion system uses the forward model simulated profiles of CO_2 concentrations mapped to OCO-2 retrieval levels ($\mathbf{f}(\mathbf{x})$) in each model grid box in order to compare with the synthetic OCO-2 observations ($\mathbf{y}$). The observation operator (M) represents the model simulated XCO_2 corresponding to each synthetic OCO-2 retrieval,

$$M = XCO_{2\,(a)} + \mathbf{a}^T(\mathbf{f}(\mathbf{x}) - \mathbf{c}_a) \quad (3)$$

using $XCO_{2\,(a)}$ and $\mathbf{c}_a$ from the retrieval (see Eq. (1)). The optimization approach used in this work defines the 4D-Var cost function (J) as,

$$J(\boldsymbol{\sigma}) = \frac{1}{2}\sum_i (M_i - \mathbf{y}_i)^T \mathbf{R}_i^{-1} (M_i - \mathbf{y}_i) + \frac{1}{2}(\boldsymbol{\sigma} - \boldsymbol{\sigma}_a)^T \mathbf{P}^{-1} (\boldsymbol{\sigma} - \boldsymbol{\sigma}_a) \quad (4)$$

where $\mathbf{y}_i$ is the vector of synthetic OCO-2 XCO_2 data across the assimilation window, with 'i' being the number of XCO_2 data. Furthermore, **R** and **P** are the observational error covariance matrix and prior error covariance matrix, respectively.

2.4.5 Prior flux uncertainty

For a perfect optimization, the prior error covariance matrix (**P**) assumed in the inversion should equal the uncertainty of the prior model used. However, the estimation of prior error statistics is a challenging task due to the lack of flux evaluation data. Previous studies have used a range of techniques to characterize prior error covariance: by developing the full error covariance matrix with assumed error correlations (Basu et al., 2013), based on a fraction of heterotrophic respiration (Basu et al., 2018), conducting Monte Carlo simulations (Liu et al., 2014), using standard deviations and absolute differences between several different prior flux models (Baker et al., 2006a; 2010), using continuous in situ measurements of CO_2 flux compared to model simulations to inform prior errors (Chevallier et al., 2006) and applying globally uniform prior flux uncertainty values to satisfy the posterior χ^2(normalized cost function) = 1 criteria (Deng et al., 2014). During this study, a 1σ standard deviation (SD) of the four prior biosphere models (see Sect. 3.1 for the description of SD values) is considered to be the measure of uncertainty in the prior knowledge of "bottom-up" model predicted biospheric CO_2 fluxes. The SD of the four prior NEE estimates is applied in the prior error covariance matrix and no spatial or temporal correlations are taken in to account. This assumption is reasonable as optimized fluxes are at coarse spatio-temporal scales (monthly mean fluxes at horizontal resolutions of > 400 km^2) and is representative of the majority of inverse modeling studies assimilating CO_2 satellite data (e.g., Baker et al., 2010; Liu et al., 2014; Deng et al., 2014). Finally, since the inverse modeling system applied in this work optimizes scaling factors, we use the square of the fractional prior error in the **P** matrix, where the fractional error is calculated for each individual prior model as the SD of the four prior models divided by the absolute value of the NEE magnitude. For generating prior error for the oceanic fluxes, we follow the same method we adopted for generating prior errors in NEE. The SD of four different state-of-the-science oceanic CO_2 flux datasets (NASA-CMS CO_2 oceanic flux from Bowman (2017), CarbonTracker 2016 prior ocean data (CT2016; http://carbontracker.noaa.gov), Takahashi et al. (2009) and Landschützer et al. (2016; 2017)) was calculated to generate prior error values.

2.4.6 XCO_2 uncertainty

As described in Sect. 2.4.3, the synthetic XCO_2 used in this study is calculated at the spatio-temporal sampling frequency of OCO-2 10-sec average dataset. Although we use synthetic XCO_2, we apply the same observation error statistics generated with the actual OCO-2 XCO_2 10-sec dataset in order to develop the observational error covariance matrix (**R**). The final observation error for the

Deleted: M_a

Deleted: $\mathbf{y}_a$

Deleted: where M_a is the prior XCO_2 used in the retrieval of the OCO-2 XCO_2 product and $\mathbf{y}_a$ is

Deleted: the corresponding prior profile of CO_2 concentrations assumed in the retrieval

10-sec average data is generated as a quadratic sum of the retrieval error from individual OCO-2 soundings, 10-sec averaging error, and a 'model representation error' as described in Basu et al. (2018). Similar to the treatment of prior error statistics, we neglect observation error correlations and assume a diagonal observational error covariance. No random perturbations were added to the synthetic XCO_2 used in this study, as the goal of this work was not to quantify the analytical posterior flux uncertainty but instead was aimed to analyze the spread among posterior NEE estimates. We note that other inverse modeling groups assimilating OCO-2 data also do not add random perturbations to the data and use the same error statistics generated along with the OCO-2 10-sec product that are applied in this study (e.g., Basu et al., 2018; Crowell et al., 2019). During this study the square of the observation error for the 10-sec average data was applied as the diagonal in the **R** matrix. From our initial OSSE tests it was determined that the use of 10-sec error statistics led to posterior χ^2 (normalized cost function) values that were much lower than unity. Therefore, we divided the 10-sec error values uniformly by a factor of 5 to approximately satisfy the $\chi^2 = 1$ criteria for all the OSSEs. This deflation procedure reduced the average 10-sec observational error values for LN+LG (OG) data from ~1.5 (~0.9) ppm to ~0.3 (~0.2) ppm. These procedures give more confidence to the observational data and lead to results in this study which can be assumed as the lower limit of the impact of prior model flux and uncertainty statistics in inverse model estimates.

Deleted: in prep

2.4.7 Evaluation of OSSE results

During this study, the posterior NEE values from the OSSEs are compared to the "true" fluxes to assess accuracy and also inter-compared to assess the spread in posterior estimates due to the assumed prior NEE and prior error statistics. The primary statistical parameters used to evaluate the spread in posterior NEE fluxes are the SD (hereafter the term "spread" will be used to represent SD) and range (difference between maximum and minimum in NEE). The SD/spread and range of posterior NEE estimates, when using the different prior models, will provide an understanding of the spatio-temporal residual impact of the prior models in "top down" estimates of global/regional NEE fluxes when assimilating OCO-2 data.

In order to evaluate the spatio-temporal variability of prior and posterior regional NEE fluxes, we aggregate individual model grid boxes to the TransCom-3 land regions (TransCom-3 regions illustrated in Fig. 1). To further interpret the OSSE results, we produce additional classifications of three broad hemisphere-scale TransCom-3 land regions: Northern Land (NL), Tropical Land (TL) and Southern Land (SL). TL includes Tropical South America, North Africa and Tropical Asia; SL includes South American Temperate, South Africa and Australia; and NL includes the other five land regions. The evaluation of SD and range of prior model and posterior/optimized NEE fluxes were calculated for the 11 individual TransCom-3 regions, for the three hemisphere-scale TransCom-3 regions and globally. Throughout the manuscript, seasonally-averaged prior and posterior NEE fluxes will be discussed and these seasons are presented with respect to the Northern Hemisphere.

Deleted: The

Deleted: Atmospheric Tracer Transport Model Intercomparison Project-3 (

Deleted:)

Deleted: S2

2.4.8 Pseudo data assimilations

In order to test our OSSE framework, we first run four "pseudo" experiments by conducting inverse modeling studies using "pseudo" surface observations. These test OSSE simulations were conducted for five-month assimilation windows for two separate seasons (November 2014 to March 2015 (analysis for winter, DJF) and May 2015 to September 2015 (analysis for summer, JJA)) using all four prior model NEE values separately. Simulated hourly concentrations of CO_2 for all surface grid boxes of GEOS-Chem are taken as "pseudo" surface observations. In order to check whether the model framework can converge to the "truth", a simple controlled experiment was performed assuming a very small observational data uncertainty (0.001%) and with the prior flux uncertainty set equal to the absolute magnitude of the "truth" - prior NEE (divided by the absolute value of the NEE magnitude for that respective prior model). The robustness of the flux inversions conducted in the subsequent sections is validated by the results of these "pseudo" tests. Figure S3 shows the results of the four "pseudo" tests using the four different NEE flux model

predictions as the prior information. From this figure it is apparent that, regardless of the prior NEE assumed, posterior NEEs were able to reproduce the "truth" with near perfect accuracy for all TransCom-3 regions, with the range between the posterior NEEs typically approaching ~0 PgC yr^{-1}. This test also demonstrates that a "perfect" assimilation (using uniform and dense surface data coverage, highly accurate data and known/loose prior uncertainty) is almost insensitive to the prior assumed. Having tested the robustness of our inversion setup, we feel confident in presenting the output from our OSSE framework, using synthetic OCO-2 remote-sensing data, in the following sections.

3. Results and discussion

3.1 Prior NEE fluxes

Figure 2 shows the seasonally-averaged multi-model-mean and SD of the NEE fluxes from the four prior biosphere models used in the OSSE simulations (individual prior model and "true" seasonally-averaged NEE fluxes are displayed in Fig. S4). This figure shows the main features of NEE that are expected, such as the Northern Hemispheric fall/winter maximum in R_e and summer maximum in GPP due to the seasonality of photosynthesis and respiration. Figure 2 also shows the spread of the four prior model fluxes (used as prior uncertainty), which is typically highest over the Temperate regions of the Northern Hemisphere in the spring and summer and high in the Tropical regions during all seasons (the left panel of Figure 3 shows a spatial map of the corresponding range of the four prior model fluxes). Furthermore, Fig. S5 shows the time-series of monthly-mean prior NEE fluxes, and the corresponding prior error uncertainty (error bars), for the individual prior models. From this figure it can be seen that the 1σ prior uncertainties for the global land are ~50-70% of the total NEE for the different prior models, with variability among other TransCom-3 land regions.

Table 3 displays the statistics of the prior NEE multi-model-mean and SD and range for the 11 individual TransCom-3 land regions. The SD values for prior NEE fluxes range from ~20% to frequently > 100% of the multi-model NEE mean for different regions/seasons with significant NEE fluxes (hereafter this refers to regions/seasons with NEE flux ≥ 0.5 PgC yr^{-1}). When comparing the magnitude of NEE between the four prior models, it can be seen from this table that the range in NEE values are large in some regions (up to 6 PgC yr^{-1}). In general, all regions/seasons tend to have at least an ~1 PgC yr^{-1} range among the four prior models, indicating the large diversity in NEE predicted by current "bottom-up" biosphere models (Table 3). Figure S5 shows the time-series of monthly-mean NEE for individual prior models averaged over the globe, hemispheric-scale land regions (NL, TL, SL) and the 11 individual TransCom-3 land regions. It can be seen from this figure that the majority of the seasonality in the global NEE flux is controlled by the NL regions. Figure S5 also shows that the spread in prior NEE fluxes in general is larger for TL and SL regions compared to the NL, except for the North American Temperate region. Furthermore, when focusing on individual models, differences in NEE seasonality are evident. The impact of these differences among the four prior biospheric CO_2 flux models on simulated XCO_2 and posterior estimates of global/regional NEE fluxes is evaluated in the following sections.

3.2 Simulated XCO_2

Figure 4 shows the number of observations sampled in the OCO-2 LN and LG modes during the different seasons of 2015 summed in each model grid box. Large spatio-temporal variability can be seen in the OCO-2 observation density, with the largest values over regions with minimal cloud coverage (e.g., desert regions of North/South Africa, Middle East, Australia, etc.). The opposite is true for many Tropical regions (e.g., Amazon, central Africa, Tropical Asia, etc.) where cloud occurrence is prominent and the number of OCO-2 observations is lowest. From Fig. 4 it can also be seen that the OCO-2 observation density has noticeable seasonality. For example, during the winter months low numbers of OCO-2 observations are made in the Northern Boreal regions

Deleted: 1
Deleted: 1
Deleted: S5
Deleted: S6
Deleted: S6
Deleted: S6
Deleted: 2
Deleted: 2

and the largest amounts are observed during the summer. Furthermore, larger numbers of OCO-2 observations are made in the SL during the summer (JJA) compared to other seasons.

The seasonally-averaged multi-model-mean GEOS-Chem simulated XCO_2 using the four prior model NEE fluxes is shown in the right panel of Fig. 4. The most notable feature in this figure is the Northern Hemisphere seasonality, with higher XCO_2 concentrations in the winter months and lowest XCO_2 values in the growing seasons of the summer. Seasonality in model-predicted XCO_2 values is also evident in the TL and SL, with largest values in the autumn and lowest values in the spring. Figure 5 (left panel) shows the range of XCO_2 values simulated using the four prior model NEE fluxes. The differences between individual model simulations of XCO_2 values deviated among themselves by up to ~10 ppm. These large differences in XCO_2 values across the four different prior NEE flux models show that the choice of prior NEE has a large impact on simulated XCO_2 values.

3.3 Optimized global NEE fluxes

From Table 1 it can be seen that annual global mean posterior NEE flux, when using the different prior models and assimilating synthetic LN+LG OCO-2 XCO_2, ranges from -4.11 to -4.36 PgC yr^{-1}, which are generally close in magnitude to the "true" flux of -4.31 PgC yr^{-1}. Although these posterior NEEs generally converged to the "truth", there are some remaining differences, with an annual global mean posterior NEE range of 0.25 PgC yr^{-1} (~6% of the multi-model-mean posterior NEE; Table 1). From the results of the OSSE simulations, it was found that the spread and range in XCO_2 simulated using the optimized posterior NEE fluxes was greatly reduced compared to the spread in XCO_2 simulated using prior NEE fluxes. This is evident from the right panel of Fig. 5 where XCO_2 simulated using posterior NEE fluxes differ among themselves by < 0.5 ppm, which is greater than an order of magnitude lower, on average, than the spread among XCO_2 simulated using prior NEEs.

Figure 3 shows the spatial distribution of the range of prior and posterior NEEs. As expected, the range in optimized posterior NEE flux estimates starting from the four separate prior models was substantially reduced compared to the spread in prior NEE fluxes. However, the posterior NEE fluxes for individual surface grid boxes of the model still depict some residual range among the posteriors, with the largest residuals being found across South America and South Africa in all seasons and in Temperate regions of the Northern Hemisphere in the spring months. As shown in Fig. 3, the geographical pattern of the range of prior and posterior NEEs does not indicate any noticeable correlations. From comparing Figs. 3 and 5, it is apparent that the spread in posterior XCO_2 is significantly reduced in all regions of the globe compared to prior model simulations, however, while posterior NEE values are reduced compared to the prior, noticeable residual spread remains in some regions. This emphasizes the fact that the OSSEs successfully converge to match the synthetic OCO-2 XCO_2 values by optimizing NEE in different ways depending on the prior NEE model used. The following sections investigate the regional differences in posterior NEE estimates due to the residual impact of prior biospheric CO_2 flux predictions.

3.4 Optimized regional NEE fluxes

Figure 6 shows the seasonally-averaged "true", prior and posterior NEE flux values for the 11 individual TransCom-3 land regions (with detailed statistics in Table 3 and monthly-mean time-series in Fig. S6). The first thing noticed from this figure is that all posterior NEE values, using variable priors, tend to reproduce the "truth" in most TransCom-3 land regions. From Fig. 6 it can also be seen that the assimilation of synthetic OCO-2 LN+LG XCO_2 retrievals resulted in a large reduction in the range among the four modeled NEE values (Table 3 shows the corresponding SD values). The reduction in the SD of NEE (also known as uncertainty reduction) in most regions/seasons, calculated as 100 × (1 – (posterior NEE SD)/(prior NEE SD)) is generally > 70% and up to 98%. However, the range of seasonal mean posterior NEEs over individual TransCom-3 regions is still as large as 1.4 PgC yr^{-1} when applying different prior NEE, with the largest ranges occurring in Northern Boreal regions (North America Boreal,

Deleted: 2
Deleted: S7
Deleted:
Deleted: S7
Deleted: S5
Deleted: S5
Deleted: S5
Deleted: S7
Deleted: 3
Deleted: S8
Deleted: 3

Eurasian Boreal and Europe) in winter months. During the spring and summer months, regions in the TL (e.g., Tropical Asia) and SL (e.g., South American Temperate, South Africa) have ranges in posterior NEEs up to ~0.5 PgC yr^{-1}. The larger residual range among posterior NEE estimates for winter months in Northern Boreal regions is likely due to the insufficient OCO-2 observations during this time (see Fig. 4), while the larger range in the TL and SL regions is due to differences in the priors (see Fig. 2). This demonstrates that the impact from the prior model has regional and seasonal variability depending on: 1) the spatio-temporal flux variabilities inherent in prior NEEs and 2) the observation density and coverage of synthetic OCO-2 data. Figure 6 and Table 3 show that the seasonally-averaged posterior NEE spread varies from ~10% to ~50% of the multi-model-mean for different TransCom-3 land regions with significant NEE fluxes. When evaluating this residual spread in posterior NEEs on a global average, seasonally-averaged values ranged from ~10% (JJA) to ~20% (DJF) of the posterior NEE mean. These statistics reveal that the impact of prior models lead to a much larger spread/range for regional/seasonal posterior fluxes (up to ~50%) compared to annual global averaged values (6%). This emphasizes that while OCO-2 observations on average constrain global, hemispheric and regional biospheric fluxes, noticeable residual differences in posterior NEE flux estimates remain due to the choice of prior model values. Overall, the results of this evaluation suggest that when inter-comparing inverse model results assimilating similar OCO-2 observational data, differences in posterior NEE in regions with significant NEE fluxes could vary by up to ~50% when using different prior flux assumptions.

3.5 Impact of prior uncertainty

Results of this study have demonstrated the sensitivity of posterior NEE estimates to prior NEE flux assumptions. In this section, the sensitivity of posterior NEE estimates to the assumed prior uncertainty is tested, when assimilating synthetic OCO-2 LN+LG XCO_2 observations. The general importance of prior uncertainty values is highlighted in the TL regions. In these regions the largest differences in prior models are calculated, thus largest prior uncertainty is assigned, resulting in larger deviations from the prior and posterior NEE spread similar to other TransCom-3 land regions (see Fig. 6). In order to quantify the sensitivity of posterior NEE to prior uncertainty statistics, a single prior NEE flux model (CASA-GFED) is applied in the OSSE framework, with variable prior flux uncertainty assumptions. Two additional OSSE simulations (in addition to the baseline simulations using the SD of the four prior models as the prior uncertainty; see right panel of Fig. 2 for SD maps) are performed using prior NEE magnitudes from CASA-GFED and setting the prior uncertainty uniformly as 10% and 100% of the CASA-GFED NEE values. Figure 7 shows the results of these additional OSSE simulations over the TransCom-3 land regions. From this figure it can be seen that the range of seasonal mean posterior NEEs over individual TransCom-3 regions vary from ~0.1 to > 1 PgC yr^{-1} when applying variable prior error assumptions. Seasonally-averaged posterior NEE SD varies from ~10-50% of the multi-model-mean for different TransCom-3 land regions with significant NEE fluxes. On a global average, seasonal-average SD values range from ~15% (JJA) to ~30% (DJF) of the posterior NEE mean. Note that these posterior NEE SD/range values here are similar to the baseline OSSEs conducted by changing prior NEE flux magnitudes (see Fig. 6). However, when comparing Fig. 7 and 6 (and Fig. S7), it is noticed that posterior NEE estimates are more sensitive to prior error assumptions compared to prior flux values in some seasons/regions of TL and SL (e.g., Northern Africa, Southern Africa, South America Temperate). It appears that NEE estimates during this study are more sensitive to prior error assumptions when sufficient observations are available and large differences between the prior and "truth" are present. Also, from Fig. 7 it can be seen that prior uncertainty assumptions in the baseline runs (using SD of prior models) and the assumption of 100% prior uncertainty tend to reproduce the "truth" more accurately than NEE estimates using 10% prior error. Overall, the results demonstrate that the posterior NEE fluxes over TransCom-3 land regions are in general similarly sensitive (up to ~50%) to the specification of prior flux uncertainties and the choice of bottom-up prior biospheric NEE model estimates.

Deleted: 2
Deleted: 1
Deleted: 3
Deleted: thus far
Deleted: 3
Deleted: 1
Deleted: 4
Deleted: 3
Deleted: 4
Deleted: 3
Deleted: S9
Deleted: 4

3.6 OCO-2 ocean data

This portion of the study investigates the impact of assimilating OCO-2 OG XCO_2 data on posterior NEE flux estimates in our OSSE framework. To do this, four additional OSSE simulations were conducted with the four prior model NEEs when only assimilating synthetic OG retrievals (instead of LN+LG) in the inversions (everything else remains the same as in the baseline simulations). Figure 8 shows the results of these four additional OSSE simulations averaged over the TransCom-3 land regions. From these simulations it can be seen that OCO-2 OG indeed reduces the range in posterior NEE flux estimates, when applying different priors, compared to prior model predictions, and can generally reproduce the "truth". On average, the spread in posterior NEE fluxes is ~20% to ~50% of the multi-model-mean for different TransCom-3 land regions with significant NEE fluxes. As expected, the comparison of Fig. 6 and 8 suggests that LN+LG data is better able to constrain biospheric CO_2 fluxes compared to OG data, as the spread among the posteriors is generally lower in LN+LG only assimilations (~70% lower on a global average) compared to OG data only assimilations. However, there were some cases where OSSE simulations using OCO-2 OG data alone did in fact result in slightly lower posterior NEE spreads in some TransCom-3 land regions compared to LN+LG assimilations runs (e.g., Northern Boreal regions during summer months and Australia during winter months). Overall, our OSSE simulations using the OCO-2 OG data demonstrate the importance of these oceanic retrievals to constrain land NEE fluxes, as the posterior NEE range is much lower compared to prior NEE estimates (see Fig. 8). This generally agrees with previous studies that demonstrated the importance of satellite data over the ocean in constraining NEE fluxes over land regions (e.g., Deng et al., 2016).

Deleted: 5

Deleted: 3

Deleted: 5

Deleted: 5

4. Conclusions

To the best of our understanding, this is the first study directly quantifying the impact of different prior global land biosphere models on the estimate of terrestrial CO_2 fluxes when assimilating OCO-2 satellite observations. We conducted a series of OSSEs that assimilated synthetic OCO-2 observations applying four state-of-the-science biospheric CO_2 flux models as the prior information. These controlled experiments were designed to systematically assess the impact of prior NEE fluxes and the impact of prior error assumptions on "top down" NEE estimates using OCO-2 data. The OSSEs incorporated NEE fluxes from the NASA-CASA, CASA-GFED, SiB-4 and LPJ biosphere models as prior estimates and variable prior flux error assumptions.

We found that the assimilation of synthetic OCO-2 XCO_2 retrievals resulted in posterior monthly/seasonal NEE estimates that generally reproduced the assumed "true" NEE globally and regionally. However, spread in posterior NEE exists in regions during seasons with poor data coverage, such as the Northern Boreal regions and some of the Tropical and Southern Hemispheric regions (e.g., South American Temperate, South Africa, Tropical Asia). This spread among posterior NEEs is likely due to the insufficient OCO-2 observations during winter over Northern Boreal regions and the large range among the priors in some of the Northern Boreal, Tropical and Southern Hemispheric regions. Residual spread from ~10% to 50% in seasonally-averaged posterior NEEs in TransCom-3 land regions with significant NEE flux were calculated due to using different prior models in inverse model simulations. We also found similar spreads in the magnitudes of posterior NEEs by conducting additional OSSEs using a single prior NEE flux model with variable prior flux uncertainty assumptions. While the spread in posterior NEE estimates, when using variable prior error statistics, was similar to when applying variable NEE flux models, the impact was larger in some seasons in the TL and SL regions. We determined that while OCO-2 observations on average constrain global, hemispheric and regional biospheric fluxes, noticeable residual differences (up to ~20-30% globally and 50% regionally) in seasonally-averaged posterior NEE flux estimates remain that were caused by the choice of prior model values and the specification of prior flux uncertainties.

There have been previous studies that investigated similar scientific objectives, such as the impact of prior uncertainties on inverse model estimates of NEE (Gurney et al., 2003; Chevalier et al., 2005; Baker et al., 2006a; 2010). The sensitivity of CO_2 flux inversions to the specification of prior flux information was first assessed by Gurney et al. (2003) using ground-based in situ

data. One main conclusion from Gurney et al. (2003) is that CO_2 flux estimates were sensitive to the prior flux uncertainty over regions with limited observations and insensitive over data-rich regions. Chevallier et al. (2005) suggested the importance of an accurate formulation of prior flux uncertainty by conducting 4D-Var assimilation of satellite column retrievals of CO_2. Baker et al. (2010) investigated the importance of assumed prior flux uncertainties by conducting sensitivity tests that mistuned the assimilations by using incorrect prior flux errors. Finally, Baker et al. (2006a, 2010) suggested the need for realistic prior models in the 4D-Var assimilations using OCO synthetic satellite CO_2 data. The results of this research are generally consistent with the findings of these past studies. However, in comparison with these previous efforts, our study is a step forward, because we quantify the specific impact of prior model NEE spatio-temporal magnitude and prior uncertainties in optimizing regional and seasonal NEEs using satellite data in a more controlled manner by applying an OSSE framework.

As explained earlier in this study, estimates of surface CO_2 fluxes from numerous inversion systems in the OCO-2 MIP ensemble model framework, using identical OCO-2 observations, result in different optimized/posterior regional NEE fluxes (Crowell et al., 2019). This inverse model variance can be due to numerous factors (e.g., model transport, inversion methods, observation errors, etc.) including prior model mean and uncertainty estimates. In order to estimate the amount of variance in the results of posterior NEE values from the OCO-2 MIP which could be due to prior flux estimates, we compare our OSSE derived residual posterior NEE range (using LN+LG) to the range in the posterior Level-4 OCO-2 Flux data (using both LN and LG) (https://www.esrl.noaa.gov/gmd/ccgg/OCO2/index.php) in each TransCom-3 region. This comparison suggests that prior NEE and uncertainty statistics could contribute 10-30% (average ~20%) of annually-averaged NEE variance calculated for each TransCom-3 region in the OCO-2 Level-4 MIP flux data. Comparing this contribution of prior model impact to the OSSE study by Basu et al. (2018), which calculated the impact of atmospheric transport on posterior NEE estimates when assimilating OCO-2 observations, this contribution is ~50% less compared to the impact of atmospheric transport. From our study and Basu et al. (2018) it is estimated that the combination of prior flux/uncertainty assumptions and atmospheric transport could contribute on average ~50% of the annually-averaged posterior NEE variance of the OCO-2 MIP study.

The results of this study suggest the need to be aware of the residual impact from prior assumptions for CO_2 global flux inversions, especially for regions and times 1) where current "bottom-up" biosphere models diverge greatly and 2) without sufficient observational coverage from space-borne platforms. For example, larger spread in posterior NEE estimates were calculated in portions of the Northern Boreal regions that tend to have insufficient satellite data coverage and moderate differences among prior biosphere models. In addition to these Northern Boreal regions, Tropical and Southern Hemispheric regions with large spread among prior biosphere models, which are assigned higher prior uncertainty values resulting in largely reduced spreads in posterior NEE estimates (large deviation from the prior), still have residual impact from the prior NEE predictions regardless of the fact that OCO-2 data is dense in these regions. Results of this study also indicate that in some regions/seasons of the TL and SL, inverse model estimates of NEE can be more sensitive to prior error statistics compared to prior flux values. Overall, in data-poor regions/times, posterior estimates from inversion techniques relying on Bayesian statistics can result in similar estimates to the prior flux, however, with some improvements over broader regions. Additionally, in regions/seasons where uncertainty in NEE fluxes are large (e.g., in the TL where prior model NEE differences are large), inverse model estimates, applying large prior uncertainty values, will still have some residual impact from the choice of prior NEE flux. Finally, care should be given when interpreting flux estimates constrained with real OCO-2 satellite data over some of the regions identified in this study as it is suggested here that residual differences (up to ~20-30% globally and 50% regionally) in seasonal posterior NEE flux estimates can be produced by the choice of prior model values and the specification of prior flux uncertainties. Finally, the results of this study suggest that multi-inverse model inter-comparison studies should consider the differences in posterior NEE flux estimates caused by variable prior fluxes and error statistics used in different models.

Deleted: In the future, studies should be designed to determine the relative importance of prior flux magnitudes and error assumptions on posterior estimates, in comparison with other error sources in inverse flux estimates (such as transport model errors and observation errors). …

5. Code and Data Availability

The forward and inverse model simulations for this work were performed using the GEOS-Chem model which is publicly available at: http://acmg.seas.harvard.edu/geos/. The 10-sec OCO-2 data used to produce synthetic observations during this study are available by request from the OCO-2 Science Team and individual OCO-2 sounding data can be downloaded here: https://oco.jpl.nasa.gov/.

6. Author Contributions

SP and MJ designed the methods and experiments presented in the study and analyzed results. CP, VG, DB, KH and BP were instrumental in providing biosphere model and OCO-2 data and guidance when applying these products. DH, JL and DB provided components implemented in the modeling framework applied during this study. Finally, SP prepared the manuscript with contributions from all listed coauthors.

Acknowledgements

Sajeev Philip's research was supported by an appointment to the NASA Postdoctoral Program at the NASA Ames Research Center, administered by Universities Space Research Association under contract with NASA. Sajeev Philip acknowledges partial support from NASA Academic Mission Services by Universities Space Research Association at NASA Ames Research Center. Daven K. Henze recognizes support from NA14OAR4310136. Resources supporting this work were provided by the NASA High-End Computing Program through the NASA Advanced Supercomputing Division at NASA Ames Research Center. We thank the OCO-2 Science Team for providing the version 8 OCO-2 product. We also thank the OCO-2 Flux Inversion Team, GEOS-Chem model developers, CASA-GFED team and NASA Carbon Monitoring System program for the free availability of their products. CarbonTracker CT2016 prior and posterior ocean fluxes were provided by National Oceanographic and Atmospheric Administration's Earth System Research Laboratory, Boulder, Colorado, USA from the website at http://carbontracker.noaa.gov. We are thankful to Sourish Basu, Feng Deng, Ray Nassar and Tom Oda for sharing data. We thank the support from the Earth Science Division of NASA Ames Research Center. The views, opinions and findings contained in this report are those of the authors and should not be construed as an official NASA or United States Government position, policy, or decision.

Deleted: DKH

References

Baker, D. F., Doney, S. C., and Schimel, D. S.: Variational data assimilation for atmospheric CO_2, Tellus B, 58, 359–365, https://doi.org/10.1111/j.1600-0889.2006.00218.x, 2006a.

Baker, D. F., Law, R. M., Gurney, K. R., Rayner, P., Peylin, P., Denning, A. S., Bousquet, P., Bruhwiler, L., Chen, Y. H., Ciais, P., Fung, I. Y., Heimann, M., John, J., Maki, T., Maksyutov, S., Masarie, K., Prather, M., Pak, B., Taguchi, S., and Zhu, Z.: TransCom 3 inversion intercomparison: Impact of transport model errors on the interannual variability of regional CO_2 fluxes, 1988–2003, Global Biogeochem. Cy., 20, GB1002, https://doi.org/10.1029/2004gb002439, 2006b.

Baker, D. F., Bösch, H., Doney, S. C., O'Brien, D., and Schimel, D. S.: Carbon source/sink information provided by column CO_2 measurements from the Orbiting Carbon Observatory, Atmos. Chem. Phys., 10, 4145-4165, https://doi.org/10.5194/acp-10-4145-2010, 2010.

Baker, I. T., Harper, A. B., da Rocha, H. R., Denning, A. S., Araújo, A. C., Borma, L. S., Freitas, H. C., Goulden, M. L., Manzi, A. O., Miller, S. D., Nobre, A. D., Restrepo-Coupe, N., Saleska, S. R., Stöckli, R., von Randow, C., and Wofsy, S. C.: Surface

ecophysiological behavior across vegetation and moisture gradients in tropical South America, Agric. For. Meteorol., 182-183, 177-188, https://doi.org/10.1016/j.agrformet.2012.11.015, 2013.

Basu, S., Guerlet, S., Butz, A., Houweling, S., Hasekamp, O., Aben, I., Krummel, P., Steele, P., Langenfelds, R., Torn, M., Biraud, S., Stephens, B., Andrews, A., and Worthy, D.: Global CO_2 fluxes estimated from GOSAT retrievals of total column CO_2, Atmos. Chem. Phys., 13, 8695-8717, https://doi.org/10.5194/acp-13-8695-2013, 2013.

Basu, S., Baker, D. F., Chevallier, F., Patra, P. K., Liu, J., and Miller, J. B.: The impact of transport model differences on CO_2 surface flux estimates from OCO-2 retrievals of column average CO_2, Atmos. Chem. Phys., 18, 7189-7215, https://doi.org/10.5194/acp-18-7189-2018, 2018.

Bey, I., Jacob, D. J., Yantosca, R. M., Logan, J. A., Field, B. D., Fiore, A. M., Li, Q. B., Liu, H. G. Y., Mickley, L. J., and Schultz, M. G.: Global modeling of tropospheric chemistry with assimilated meteorology: Model description and evaluation, J. Geophys. Res. Atmos., 106, 23073–23095, https://doi.org/10.1029/2001JD000807, 2001.

Bowman, K. W.: Carbon Monitoring System Flux for Shipping, Aviation, and Chemical Sources L4 V1, Greenbelt, MD, USA, Goddard Earth Sciences Data and Information Services Center (GES DISC), Accessed [February 19, 2018], https://doi.org/10.5067/RLT7JTCRJ11M, 2017.

Bowman, K. W., Liu, J., Bloom, A. A., Parazoo, N. C., Lee, M., Jiang, Z., Menemenlis, D., Gierach, M. M., Collatz, G. J., Gurney, K. R., and Wunch D.: Global and Brazilian carbon response to El Niño Modoki 2011–2010, Earth and Space Sci., 4, 637–660, https://doi.org/10.1002/2016EA000204, 2017.

Byrne, B., Jones, D. B. A., Strong, K., Zeng, Z.-C., Deng, F., and Liu, J.: Sensitivity of CO_2 surface flux constraints to observational coverage, J. Geophys. Res. Atmos., 122, 6672–6694, https://doi.org/10.1002/2016JD026164, 2017.

Chevallier, F., Fisher, M., Peylin, P., Serrar, S., Bousquet, P., Bréon, F.-M., Chédin, A., and Ciais, P.: Inferring CO_2 sources and sinks from satellite observations: Method and application to TOVS data, J. Geophys. Res. Atmos., 110, D24309, https://doi.org/10.1029/2005JD006390, 2005.

Chevallier, F., Feng, L., Bösch, H., Palmer, P. I., and Rayner, P. J.: On the impact of transport model errors for the estimation of CO_2 surface fluxes from GOSAT observations, Geophys. Res. Lett., 37, L21803, https://doi.org/10.1029/2010GL044652, 2010.

Chevallier, F., Palmer, P. I., Feng, L., Bösch, H., O'Dell, C. W., and Bousquet, P.: Toward robust and consistent regional CO_2 flux estimates from in situ and spaceborne measurements of atmospheric CO_2, Geophys. Res. Lett., 41, 1065–1070, https://doi.org/10.1002/2013GL058772, 2014.

Chevallier, F., Viovy, N., Reichstein, M., and Ciais, P.: On the assignment of prior errors in Bayesian inversions of CO_2 surface fluxes, Geophys. Res. Lett., 33, L13802, https://doi.org/:10.1029/2006GL026496, 2006.

Corbett, J. J. and Koehler, H. W.: Updated emissions from ocean shipping, J. Geophys. Res. Atmos., 108(D20), 4650, https://doi.org/10.1029/2003JD003751, 2003.

Corbett, J. J. and Koehler, H. W.: Considering alternative input parameters in an activity-based ship fuel consumption and emissions model: Reply to comment by Øyvind Endresen et al. on ''Updated emissions from ocean shipping'', J. Geophys. Res. Atmos., 109, D23303, https://doi.org/10.1029/2004JD005030, 2004.

Crisp, D., Pollock, H. R., Rosenberg, R., Chapsky, L., Lee, R. A. M., Oyafuso, F. A., Frankenberg, C., O'Dell, C. W., Bruegge, C. J., Doran, G. B., Eldering, A., Fisher, B. M., Fu, D., Gunson, M. R., Mandrake, L., Osterman, G. B., Schwandner, F. M., Sun, K., Taylor, T. E., Wennberg, P. O., and Wunch, D.: The on-orbit performance of the Orbiting Carbon Observatory-2 (OCO-

Formatted: Subscript

2) instrument and its radiometrically calibrated products, Atmos. Meas. Tech., 10, 59-81, https://doi.org/10.5194/amt-10-59-2017, 2017.

Crowell, S., Baker, D., Schuh, A., Basu, S., Jacobson, A. R., Chevallier, F., Liu, J., Deng, F., Feng, L., McKain, K., Chatterjee, A., Miller, J. B., Stephens, B. B., Eldering, A., Crisp, D., Schimel, D., Nassar, R., O'Dell, C. W., Oda, T., Sweeney, C., Palmer, P. I., and Jones, D. B. A.: The 2015–2016 carbon cycle as seen from OCO-2 and the global in situ network, Atmos. Chem. Phys., 19, 9797–9831, https://doi.org/10.5194/acp-19-9797-2019, 2019.

Deng, F., Jones, D. B. A., Henze, D. K., Bousserez, N., Bowman, K. W., Fisher, J. B., Nassar, R., O'Dell, C., Wunch, D., Wennberg, P. O., Kort, E. A., Wofsy, S. C., Blumenstock, T., Deutscher, N. M., Griffith, D. W. T., Hase, F., Heikkinen, P., Sherlock, V., Strong, K., Sussmann, R., and Warneke, T.: Inferring regional sources and sinks of atmospheric CO_2 from GOSAT XCO_2 data, Atmos. Chem. Phys., 14, 3703-3727, https://doi.org/10.5194/acp-14-3703-2014, 2014.

Deng, F., Jones, D. B. A. O'Dell, C. W., Nassar, R., and Parazoo N. C.: Combining GOSAT XCO_2 observations over land and ocean to improve regional CO_2 flux estimates, J. Geophys. Res. Atmos., 121, 1896–1913, https://doi.org/10.1002/2015JD024157, 2016.

Denning, A. S., Collatz, G. J., Zhang, C., Randall, D. A., Berry, J. A., Sellers, P. J., Colello, G. D., and Dazlich, D. A.: Simulations of terrestrial carbon metabolism and atmospheric CO_2 in a general circulation model, Tellus B, 48B, 521-542, https://doi.org/10.1034/j.1600-0889.1996.t01-2-00009.x, 1996.

Eldering, A., O'Dell, C. W., Wennberg, P. O., Crisp, D., Gunson, M. R., Viatte, C., Avis, C., Braverman, A., Castano, R., Chang, A., Chapsky, L., Cheng, C., Connor, B., Dang, L., Doran, G., Fisher, B., Frankenberg, C., Fu, D., Granat, R., Hobbs, J., Lee, R. A. M., Mandrake, L., McDuffie, J., Miller, C. E., Myers, V., Natraj, V., O'Brien, D., Osterman, G. B., Oyafuso, F., Payne, V. H., Pollock, H. R., Polonsky, I., Roehl, C. M., Rosenberg, R., Schwandner, F., Smyth, M., Tang, V., Taylor, T. E., To, C., Wunch, D., and Yoshimizu, J.: The Orbiting Carbon Observatory-2: first 18 months of science data products, Atmos. Meas. Tech., 10, 549-563, https://doi.org/10.5194/amt-10-549-2017, 2017a.

Eldering, A., Wennberg, P. O., Crisp, D., Schimel, D. S., Gunson, M. R., Chatterjee, A., Liu, J., Schwandner, F. M., Sun, Y., O'Dell, C. W., Frankenberg, C., Taylor, T., Fisher, B., Osterman, G. B., Wunch, D., Hakkarainen, J., Tamminen, J., and Weir, B.: The Orbiting Carbon Observatory-2 early science investigations of regional carbon dioxide fluxes, Science, 358, eaam5745, https://doi.org/10.1126/science.aam5745, 2017b.

Fisher, J. B., Sikka, M., Huntzinger, D. N., Schwalm, C., and Liu, J.: Technical note: 3-hourly temporal downscaling of monthly global terrestrial biosphere model net ecosystem exchange, Biogeosciences, 13, 4271-4277, https://doi.org/10.5194/bg-13-4271-2016, 2016a.

Fisher, J. B., Sikka, M., Huntzinger, D. N., Schwalm, C. R., Liu, J., Wei, Y., Cook, R. B., Michalak, A. M., Schaefer, K., Jacobson, A. R., Arain, M. A., Ciais, P., El-masri, B., Hayes, D. J., Huang, M., Huang, S., Ito, A., Jain, A. K., Lei, H., Lu, C., Maignan, F., Mao, J., Parazoo, N. C., Peng, C., Peng, S., Poulter, B., Ricciuto, D. M., Tian, H., Shi, X., Wang, W., Zeng, N., Zhao, F., and Zhu, Q.: CMS: Modeled Net Ecosystem Exchange at 3-hourly Time Steps, 2004-2010, ORNL DAAC, Oak Ridge, Tennessee, USA., https://doi.org/10.3334/ORNLDAAC/1315, 2016b.

Gurney, K. R., Law, R. M., Denning, A. S., Rayner, P. J., Baker, D., Bousquet, P., Bruhwiler, L., Chen, Y.-H., Ciais, P., Fan, S., Fung, I. Y., Gloor, M., Heimann, M., Higuchi, K., John, J., Kowalczyk, E., Maki, T., Maksyutov, S., Peylin, P., Prather, M., Pak, B. C., Sarmiento, J., Taguchi, S., Takahashi, T., and Yuen, C.-W.: TransCom 3 CO_2 inversion intercomparison: 1. Annual mean control results and sensitivity to transport and prior flux information, Tellus B, 55B, 555-579, https://doi.org/10.1034/j.1600-0889.2003.00049.x, 2003.

Deleted: Crowell, S. et al.: The 2015-2016 carbon cycle as seen from OCO-2 and the global in situ network, in preparation.

Harris, I., Jones, P. D., Osborn, T. J., and Lister, D. H.: Updated high-resolution grids of monthly climatic observations – the CRU TS3.10 Dataset, Int. J. Climatol., 34, 623-642, https://doi.org/10.1002/joc.3711, 2013.

Haxeltine, A., and Prentice, I. C.: A general model for the light-use efficiency of primary production. Funct. Ecol., 10, 551-561, https://doi.org/10.2307/2390165, 1996.

Haynes, K. D., Baker, I. T., Denning, A. S., Stöckli, R., Schaefer, K., and Lokupitiya, E.: Global Self-Consistent Carbon Flux and Pool Estimates Utilizing the Simple Biosphere Model (SiB4). Abstract B31F-01 presented at 2013 AGU Fall Meeting, AGU, San Fransisco, CA, 9-13 December, 2013.

Heimann, M., Esser, G., Haxeltine, A., Kaduk, J., Kicklighter, D. W., Knorr, W., Kohlmaier, G. H., McGuire, A. D., Melillo, J., Moore III, B., Otto, R. D., Prentice, I. C., Sauf, W., Schloss, A., Sitch, S., Wittenberg, U., and Würth, G.: Evaluation of terrestrial Carbon Cycle models through simulations of the seasonal cycle of atmospheric CO_2: First results of a model intercomparison study, Global Biogeochem. Cy., 12, 1–24, https://doi.org/10.1029/97GB01936, 1998.

Henze, D. K., Hakami, A., and Seinfeld, J. H.: Development of the adjoint of GEOS-Chem, Atmos. Chem. Phys., 7, 2413-2433, https://doi.org/10.5194/acp-7-2413-2007, 2007.

Houweling, S., Aben, I., Breon, F.-M., Chevallier, F., Deutscher, N., Engelen, R., Gerbig, C., Griffith, D., Hungershoefer, K., Macatangay, R., Marshall, J., Notholt, J., Peters, W., and Serrar, S.: The importance of transport model uncertainties for the estimation of CO_2 sources and sinks using satellite measurements, Atmos. Chem. Phys., 10, 9981-9992, https://doi.org/10.5194/acp-10-9981-2010, 2010.

Houweling, S., Baker, D., Basu, S., Boesch, H., Butz, A., Chevallier, F., Deng, F., Dlugokencky, E. J., Feng, L., Ganshin, A., Hasekamp, O., Jones, D., Maksyutov, S., Marshall, J., Oda, T., O'Dell, C. W., Oshchepkov, S., Palmer, P. I., Peylin, P., Poussi, Z., Reum, F., Takagi, H., Yoshida, Y., and Zhuravlev, R.: An intercomparison of inverse models for estimating sources and sinks of CO_2 using GOSAT measurements, J. Geophys. Res. Atmos., 120, 5253–5266, https://doi.org/10.1002/2014JD022962, 2015.

Huntzinger, D. N., Post, W. M., Wei, Y., Michalak, A. M., West T. O., Jacobson, A. R., Baker, I. T., Chen, J. M., Davis, K. J., Hayes, D. J., Hoffman, F. M., Jain, A. K., Liu, S., McGuire, A. D., Neilson, R. P., Potter, C., Poulter, B., Price, D., Raczka, B. M., Tian, H., Q., Thornton, P., Tomelleri, E., Viovy, N., Xiao, J., Yuan, W., Zeng, N., Zhao, M., and Cook, R.: North American Carbon Program (NACP) regional interim synthesis: Terrestrial biospheric model intercomparison, Ecol. Model., 232, 144-157, https://doi.org/10.1016/j.ecolmodel.2012.02.004, 2012.

Huntzinger, D. N., Schwalm, C., Michalak, A. M., Schaefer, K., King, A. W., Wei, Y., Jacobson, A., Liu, S., Cook, R. B., Post, W. M., Berthier, G., Hayes, D., Huang, M., Ito, A., Lei, H., Lu, C., Mao, J., Peng, C. H., Peng, S., Poulter, B., Riccuito, D., Shi, X., Tian, H., Wang, W., Zeng, N., Zhao, F., and Zhu, Q.: The North American Carbon Program Multi-Scale Synthesis and Terrestrial Model Intercomparison Project – Part 1: Overview and experimental design, Geosci. Model Dev., 6, 2121-2133, https://doi.org/10.5194/gmd-6-2121-2013, 2013.

Huntzinger, D. N., Schwalm, C. R., Wei, Y., Cook, R. B., Michalak, A. M., Schaefer, K., Jacobson, A. R., Arain, M. A., Ciais, P., Fisher, J. B., Hayes, D. J., Huang, M., Huang, S., Ito, A., Jain, A. K., Lei, H., Lu, C., Maignan, F., Mao, J., Parazoo, N. C., Peng, C., Peng, S., Poulter, B., Ricciuto, D. M., Tian, H., Shi, X., Wang, W., Zeng, N., Zhao, F., Zhu, Q., Yang, J., and Tao, B.: NACP MsTMIP: Global 0.5-degree Model Outputs in Standard Format, Version 1.0. ORNL DAAC, Oak Ridge, Tennessee, USA. https://doi.org/10.3334/ORNLDAAC/1225, 2018.

IPCC, 2014: Climate Change 2014: Synthesis Report. Contribution of Working Groups I, II and III to the Fifth Assessment Report of the Intergovernmental Panel on Climate Change [Core Writing Team, R.K. Pachauri and L.A. Meyer (eds.)], IPCC, Geneva, Switzerland, 151 pp, 2014.

Ito, A., Inatomi, M., Huntzinger, D. N., Schwalm, C., Michalak, A. M., Cook, R., King, A. W., Mao, J., Wei, Y., Post, W. M., Wang, W., Arain, M. A., Huang, S., Hayes, D. J., Ricciuto, D. M., Shi, X., Huang, M., Lei, H., Tian, H., Lu, C., Yang, J., Tao, B., Jain, A., Poulter, B., Peng, S., Ciais, P., Fisher, J. B., Parazoo, N. C., Schaefer, K., Peng, C., Zeng, N., and Zhao, F.: Decadal trends in the seasonal-cycle amplitude of terrestrial CO_2 exchange resulting from the ensemble of terrestrial biosphere models, Tellus B, 68, 28968, https://doi.org/10.3402/tellusb.v68.28968, 2016.

Landschützer, P., Gruber, N., and Bakker, D. C. E.: Decadal variations and trends of the global ocean carbon sink, Global Biogeochem. Cy., 30, 1396–1417, https://doi.org/10.1002/2015GB005359, 2016.

Landschützer, P., Gruber, N., and Bakker, D. C. E.: An updated observation-based global monthly gridded sea surface pCO_2 and air-sea CO_2 flux product from 1982 through 2015 and its monthly climatology (NCEI Accession 0160558), Version 2.2, NOAA National Centers for Environmental Information, Dataset, [2017-07-11], 2017.

Law, R. M., Chen, Y-H., Gurney, K. R., and TransCom 3 modelers: TransCom 3 CO_2 inversion intercomparison: 2. Sensitivity of annual mean results to data choices, Tellus B, 55B, 580-595, https://doi.org/10.1034/j.1600-0889.2003.00053.x, 2003.

Le Quéré, C., Andrew, R. M., Friedlingstein, P., Sitch, S., Pongratz, J., Manning, A. C., Korsbakken, J. I., Peters, G. P., Canadell, J. G., Jackson, R. B., Boden, T. A., Tans, P. P., Andrews, O. D., Arora, V. K., Bakker, D. C. E., Barbero, L., Becker, M., Betts, R. A., Bopp, L., Chevallier, F., Chini, L. P., Ciais, P., Cosca, C. E., Cross, J., Currie, K., Gasser, T., Harris, I., Hauck, J., Haverd, V., Houghton, R. A., Hunt, C. W., Hurtt, G., Ilyina, T., Jain, A. K., Kato, E., Kautz, M., Keeling, R. F., Klein Goldewijk, K., Körtzinger, A., Landschützer, P., Lefèvre, N., Lenton, A., Lienert, S., Lima, I., Lombardozzi, D., Metzl, N., Millero, F., Monteiro, P. M. S., Munro, D. R., Nabel, J. E. M. S., Nakaoka, S.-I., Nojiri, Y., Padin, X. A., Peregon, A., Pfeil, B., Pierrot, D., Poulter, B., Rehder, G., Reimer, J., Rödenbeck, C., Schwinger, J., Séférian, R., Skjelvan, I., Stocker, B. D., Tian, H., Tilbrook, B., Tubiello, F. N., van der Laan-Luijkx, I. T., van der Werf, G. R., van Heuven, S., Viovy, N., Vuichard, N., Walker, A. P., Watson, A. J., Wiltshire, A. J., Zaehle, S., and Zhu, D.: Global Carbon Budget 2017, Earth Syst. Sci. Data, 10, 405-448, https://doi.org/10.5194/essd-10-405-2018, 2018.

Liu, D. C., and Nocedal J.: On the limited memory BFGS method for large scale optimization, Math. Prog., 45, 503-528, https://doi.org/10.1007/bf01589116, 1989.

Liu, J., Bowman, K. W., Lee, M., Henze, D. K., Bousserez, N., Brix, H., Collatz, G. J., Menemenlis, D., Ott, L., Pawson, S., Jones, D., and Ray Nassar, R.: Carbon monitoring system flux estimation and attribution: impact of ACOS-GOSAT XCO_2 sampling on the inference of terrestrial biospheric sources and sinks, Tellus B, 66, 22486, https://doi.org/10.3402/tellusb.v66.22486, 2014.

Liu, J., Bowman, K. W., Schimel, D. S., Parazoo, N. C., Jiang, Z., Lee, M., Bloom, A. A., Wunch, D., Frankenberg, C., Sun, Y., O'Dell, C. W., Gurney, K. R., Menemenlis, D., Gierach, M., Crisp, D., and Eldering A.: Contrasting carbon cycle responses of the tropical continents to the 2015–2016 El Niño, Science, 358, eaam5690, https://doi.org/10.1126/science. aam5690, 2017.

Lokupitiya, E., Denning, A. S., Paustian, K., Baker, I., Schaefer, K., Verma, S., Meyers, T., Bernacchi, C. J., Suyker, A., and Fischer, M.: Incorporation of crop phenology in Simple Biosphere Model (SiBcrop) to improve land-atmosphere carbon exchanges from croplands, Biogeosciences, 6, 969-986, https://doi.org/10.5194/bg-6-969-2009, 2009.

Nassar, R., Jones, D. B. A., Suntharalingam, P., Chen, J. M., Andres, R. J., Wecht, K. J., Yantosca, R. M., Kulawik, S. S., Bowman, K. W., Worden, J. R., Machida, T., and Matsueda, H.: Modeling global atmospheric CO_2 with improved emission inventories

and CO_2 production from the oxidation of other carbon species, Geosci. Model Dev., 3, 689-716, https://doi.org/10.5194/gmd-3-689-2010, 2010.

Nassar, R., Napier-Linton, L., Gurney, K. R., Andres, R. J., Oda, T., Vogel, F. R., and Deng, F.: Improving the temporal and spatial distribution of CO_2 emissions from global fossil fuel emission data sets, J. Geophys. Res. Atmos., 118, 917–933, https://doi.org/10.1029/2012JD018196, 2013.

Oda, T., Maksyutov, S., and Andres, R. J.: The Open-source Data Inventory for Anthropogenic CO_2, version 2016 (ODIAC2016): a global monthly fossil fuel CO_2 gridded emissions data product for tracer transport simulations and surface flux inversions, Earth Syst. Sci. Data, 10, 87-107, https://doi.org/10.5194/essd-10-87-2018, 2018.

O'Dell, C. W., Connor, B., Bösch, H., O'Brien, D., Frankenberg, C., Castano, R., Christi, M., Eldering, D., Fisher, B., Gunson, M., McDuffie, J., Miller, C. E., Natraj, V., Oyafuso, F., Polonsky, I., Smyth, M., Taylor, T., Toon, G. C., Wennberg, P. O., and Wunch, D.: The ACOS CO_2 retrieval algorithm – Part 1: Description and validation against synthetic observations, Atmos. Meas. Tech., 5, 99-121, https://doi.org/10.5194/amt-5-99-2012, 2012.

Olsen, S. C. and Randerson, J. T.: Differences between surface and column atmospheric CO_2 and implications for carbon cycle research, J. Geophys. Res. Atmos., 109, D02301, https://doi.org/10.1029/2003JD003968, 2004.

Olsen, S. C., Wuebbles, D. J., and Owen, B.: Comparison of global 3-D aviation emissions datasets, Atmos. Chem. Phys., 13, 429-441, https://doi.org/10.5194/acp-13-429-2013, 2013.

Ott, L. E., Pawson, S., Collatz, G. J., Gregg, W. W., Menemenlis, D., Brix, H., Rousseaux, C. S., Bowman, K. W., Liu, J., Eldering, A., Gunson, M. R., and Kawa, S. R.: Assessing the magnitude of CO_2 flux uncertainty in atmospheric CO_2 records using products from NASA's Carbon Monitoring Flux Pilot Project, J. Geophys. Res. Atmos., 120,734–765, https://doi.org/10.1002/2014JD022411, 2015.

Peng, S., Ciais, P., Chevallier, F., Peylin, P., Cadule, P., Sitch, S., Piao, S., Ahlström, A., Huntingford, C., Levy, P., Li, X., Liu, Y., Lomas, M., Poulter, B., Viovy, N., Wang, T., Wang, X., Zaehle, S., Zeng, N., Zhao, F., and Zhao, H.: Benchmarking the seasonal cycle of CO_2 fluxes simulated by terrestrial ecosystem models, Global Biogeochem. Cy., 29, 46–64, https://doi.org/10.1002/2014GB004931, 2015.

Peylin, P., Law, R. M., Gurney, K. R., Chevallier, F., Jacobson, A. R., Maki, T., Niwa, Y., Patra, P. K., Peters, W., Rayner, P. J., Rödenbeck, C., van der Laan-Luijkx, I. T., and Zhang, X.: Global atmospheric carbon budget: results from an ensemble of atmospheric CO_2 inversions, Biogeosciences, 10, 6699-6720, https://doi.org/10.5194/bg-10-6699-2013, 2013.

Peters, W., Jacobson, A. R., Sweeney, C., Andrews, A. E., Conway, T. J., Masarie, K., Miller, J. B., Bruhwiler, L. M. P., Pétron, G., Hirsch, A. I., Worthy, D. E. J., van der Werf, G. R., Randerson, J. T., Wennberg, P. O., Krol, M. C., and Tans, P. P.: An atmospheric perspective on North American carbon dioxide exchange: CarbonTracker, Proc. Natl. Acad. Sci., 104, 18925–18930, https://doi.org/10.1073/pnas.0708986104, 2007.

Potter, C., Randerson, J. T., Field, C. B., Matson, P. A., Vitousek, P. M., Mooney, H. A., and Klooster, S A.: Terrestrial ecosystem production: A process model based on global satellite and surface data, Global Biogeochem. Cy., 7, 811-841, https://doi.org/10.1029/93GB02725, 1993.

Potter, C., Klooster, S., Myneni, R., Genovese, V., Tan, P.-N., and Kumar, V.: Continental scale comparisons of terrestrial carbon sinks estimated from satellite data and ecosystem modeling 1982-98, Glob. Planet. Chang., 39, 201-213, https://doi.org/10.1016/j.gloplacha.2003.07.001, 2003.

Potter, C., Kumar, V., Klooster, S., and Nemani, R.: Recent history of trends in vegetation greenness and large-scale ecosystem disturbances in Eurasia, Tellus B, 59, 260-272, https://doi.org/10.1111/j.1600-0889.2006.00245.x, 2007.

Potter, C., Klooster, S., Huete, A., Genovese, V., Bustamante, M., Guimaraes Ferreira, L., R. C. de Oliveira Jr., and Zepp, R.: Terrestrial carbon sinks in the Brazilian Amazon and Cerrado region predicted from MODIS satellite data and ecosystem modeling, Biogeosciences, 6, 937-945, https://doi.org/10.5194/bg-6-937-2009, 2009.

Potter, C., Klooster, S., and Genovese, V.: Net primary production of terrestrial ecosystems from 2000 to 2009, Climatic Change, 115, 365-378, http://dx.doi.org/10.1007/s10584-012-0460-2, 2012a.

Potter, C., Klooster, S., Genovese, V., Hiatt, C., Boriah, S., Kumar, V., Mithal, V., and Garg, A.: Terrestrial ecosystem carbon fluxes predicted from MODIS satellite data and large-scale disturbance modeling, Int. J. Geosci., 3, 469-479, http://dx.doi.org/10.4236/ijg.2012.33050, 2012b.

Poulter, B., Frank, D., Ciais, P., Myneni, R. B., Andela, N., Bi, J., Broquet, G., Canadell, J. G., Chevallier, F., Liu, Y. Y., Running, S. W., Sitch, S., and van der Werf, G. R.: Contribution of semi-arid ecosystems to interannual variability of the global carbon cycle, Nature, 509, 600–603, http://dx.doi.org/10.1038/nature13376, 2014.

Randerson, J. T., Thompson, M. V., Malmstrom, C. M., Field, C. B., and Fung, I. Y.: Substrate limitations for heterotrophs: Implications for models that estimate the seasonal cycle of atmospheric CO_2, Global Biogeochem. Cy., 10,, 585–602, https://doi.org/10.1029/96GB01981, 1996.

Rödenbeck, C., Houweling, S., Gloor, M., and Heimann, M.: CO_2 flux history 1982–2001 inferred from atmospheric data using a global inversion of atmospheric transport, Atmos. Chem. Phys., 3, 1919-1964, https://doi.org/10.5194/acp-3-1919-2003, 2003.

Rödenbeck, C., Conway, T. J., and Langenfelds, R. L.: The effect of systematic measurement errors on atmospheric CO_2 inversions: a quantitative assessment, Atmos. Chem. Phys., 6, 149-161, https://doi.org/10.5194/acp-6-149-2006, 2006.

Schaefer, K., Collatz, G. J., Tans, P., Denning, A. S., Baker, I., Berry, J., Prihodko, L., Suits, N., and Philpott, A.: Combined Simple Biosphere/Carnegie-Ames-Stanford Approach terrestrial carbon cycle model, J. Geophys. Res. Biogeosci., 113, G03034, https://doi.org/10.1029/2007JG000603, 2008.

Schimel, D. S., House, J. I., Hibbard, K. A., Bousquet, P., Ciais, P., Peylin, P., Braswell, B. H., Apps, M. J., Baker, D., Bondeau, A., Canadell, J., Churkina, G., Cramer, W., Denning, A. S., Field, C. B., Friedlingstein, P., Goodale, C., Heimann, M., Houghton, R. A., Melillo, J. M., Moore III, B., Murdiyarso, D., Noble, I., Pacala, S. W., Prentice, I. C., Raupach, M. R., Rayner, P. J., Scholes, R. J., Steffen, W. L., and Wirth, C.: Recent patterns and mechanisms of carbon exchange by terrestrial ecosystems, Nature, 414, 169-172, https://doi.org/10.1038/35102500, 2001.

Schimel, D., Stephens, B. B., and Fisher, J. B.: Effect of increasing CO_2 on the terrestrial carbon cycle, Proc. Natl. Acad. Sci., 112, 436–441, https://doi.org/10.1073/pnas.1407302112, 2015.

Schwalm, C. R., Huntzinger, D. N., Fisher, J. B., Michalak, A. M., Bowman, K., Ciais, P., Cook, R., El-Masri, B., Hayes, D., Huang, M., Ito, A., Jain, A., King, A. W., Lei, H., Liu, J., Lu, C., Mao, J., Peng, S., Poulter, B., Ricciuto, D., Schaefer, K., Shi, X., Tao, B., Tian, H., Wang, W., Wei, Y., Yang, J., and Zeng, N.: Toward “optimal” integration of terrestrial biosphere models, Geophys. Res. Lett., 42, 4418–4428, https://doi.org/10.1002/2015GL064002, 2015.

Seinfeld, J. H. and Pandis, S. N.: Atmospheric chemistry and physics: from air pollution to climate change, 3rd Edn. Wiley, 2016.

Sellers, P. J., Mintz, Y., Sud, Y. C., and Dalcher, A.: A simple biosphere model (SiB) for use within general circulation models, J. Atmos. Sci., 43, 505-531, https://doi.org/10.1175/1520-0469(1986)043<0505:ASBMFU>2.0.CO;2, 1986.

Sellers, P. J., Randall, D. A., Collatz, G. J., Berry, J. A., Field, C. B., Dazlich, D. A., Zhang, C., Collelo, G. D., and Buonoua, L.: A revised Land Surface Parameterization (SiB2) for atmospheric GCMs. Part I: Model formulation, J. Clim., 9, 676-705, https://doi.org/10.1175/1520-0442(1996)009<0676:ARLSPF>2.0.CO;2, 1996.

Sitch, S., Smith, B., Prentice, I. C., Arneth, A., Bondeau, A., Cramer, W., Kaplan, J. O., Levis, S., Lucht, W., Sykes, M. T., Thonicke, K., and Venevsky, S.: Evaluation of ecosystem dynamics, plant geography and terrestrial carbon cycling in the LPJ dynamic global vegetation model, Glob. Change Biol., 9, 161–185, https://doi.org/10.1046/j.1365-2486.2003.00569.x, 2003.

Suntharalingam, P., Jacob, D. J., Palmer, P. I., Logan, J. A., Yantosca, R. M., Xiao, Y., Evans, M. J., Streets, D. G., Vay, S. L., and Sachse, G. W.: Improved quantification of Chinese carbon fluxes using CO_2/CO correlations in Asian outflow, J. Geophys. Res. Atmos., 109, D18S18, https://doi.org/10.1029/2003JD004362, 2004.

Sitch, S., Friedlingstein, P., Gruber, N., Jones, S. D., Murray-Tortarolo, G., Ahlström, A., Doney, S. C., Graven, H., Heinze, C., Huntingford, C., Levis, S., Levy, P. E., Lomas, M., Poulter, B., Viovy, N., Zaehle, S., Zeng, N., Arneth, A., Bonan, G., Bopp, L., Canadell, J. G., Chevallier, F., Ciais, P., Ellis, R., Gloor, M., Peylin, P., Piao, S. L., Le Quéré, C., Smith, B., Zhu, Z., and Myneni, R.: Recent trends and drivers of regional sources and sinks of carbon dioxide, Biogeosciences, 12, 653-679, https://doi.org/10.5194/bg-12-653-2015, 2015.

Takagi H., Houweling, S., Andres, R. J., Belikov, D., Bril, A., Boesch H., Butz, A., Guerlet, S., Hasekamp, O., Maksyutov, S., Morino, I., Oda T., O'Dell, C. W., Oshchepkov, S., Parker, R., Saito, M., Uchino, O., Yokota, T., Yoshida, Y., and Valsala, V.: Influence of differences in current GOSAT XCO_2 retrievals on surface flux estimation, Geophys. Res. Lett., 41, 2598–2605, https://doi.org/10.1002/2013GL059174, 2014.

Takahashi, T., Sutherland, S. C., Wanninkhof, R., Sweeney, C., Feely, R. A., Chipman, D. W., Hales, B., Friederich, G., Chavez, F., Sabine, C., Watson, A., Bakker, D. C. E., Schuster, U., Metzl, N., Yoshikawa-Inoue, H., Ishii, M., Midorikawa, T., Nojiri, Y., Körtzinger, A., Steinhoff, T., Hoppema, M., Olafsson, J., Arnarson, T. S., Tilbrook, B., Johannessen, T., Olsen, A., Bellerby, R., Wong, C. S., Delille, B., Bates, N. R., and de Baar, H. J. W.: Climatological mean and decadal change in surface ocean pCO_2, and net sea-air CO_2 flux over the global oceans, Deep Sea Res. II: Topical Stud. Oceanogr., 56, 554–577, https://doi.org/10.1016/j.dsr2.2008.12.009, 2009.

van der Werf, G. R., Randerson, J. T., Collatz, G. J., Giglio, L., Kasibhatla, P. S., Arellano, A. F., Olsen, S. C., and Kasischke, E. S.: Continental-scale partitioning of fire emissions during the 1997 to 2001 El Nino/La Nina period, Science, 303, 73–76, https://doi.org/10.1126/science.1090753, 2004.

van der Werf, G. R., Randerson, J. T., Giglio, L., Collatz, G. J., Kasibhatla, P. S., and Arellano Jr., A. F.: Interannual variability in global biomass burning emissions from 1997 to 2004, Atmos. Chem. Phys., 6, 3423-3441, https://doi.org/10.5194/acp-6-3423-2006, 2006.

van der Werf, G. R., Randerson, J. T., Giglio, L., Collatz, G. J., Mu, M., Kasibhatla, P. S., Morton, D. C., DeFries, R. S., Jin, Y., and van Leeuwen, T. T.: Global fire emissions and the contribution of deforestation, savanna, forest, agricultural, and peat fires (1997–2009), Atmos. Chem. Phys., 10, 11707-11735, https://doi.org/10.5194/acp-10-11707-2010, 2010.

Wang, J. S., Kawa, S. R., Collatz, G. J., Sasakawa, M., Gatti, L. V., Machida, T., Liu, Y., and Manyin, M. E.: A global synthesis inversion analysis of recent variability in CO_2 fluxes using GOSAT and in situ observations, Atmos. Chem. Phys., 18, 11097-11124, https://doi.org/10.5194/acp-18-11097-2018, 2018.

Table 1: Prior and (Posterior) global annual mean NEE fluxes and CO_2 emission inventories (PgC yr^{-1}) for the year 2015 used in the OSSE simulations during this study.

NEE Model	NEE flux (PgC yr^{-1})
MsTMIP[1,2]	-4.31
NASA-CASA[3]	-1.86 (-4.14)
CASA-GFED[4]	-2.42 (-4.24)
SiB-4[5]	0.95 (-4.11)
LPJ[6]	-5.53 (-4.36)
Inventory	**CO_2 emission (PgC yr^{-1})**
Fossil fuel[7]	9.86
Ocean[8]	-2.41
Biomass burning[9]	2.05
Fuel wood burning[9]	0.50

[1]MsTMIP NEE dataset is representative of the year 2010 and is an ensemble mean of 15 different NEE models.
[2]Huntzinger et al., 2013; 2016; Fisher et al., 2016a,2016b
[3]Potter et al., 1993; 2012a; 2012b
[4]Potter et al., 1993; Randerson et al., 1996
[5]Haynes et al., 2013; Baker et al., 2013
[6]Sitch et al., 2003; Poulter et al., 2014
[7]Oda et al., 2018; Nassar et al., 2013
[8]CarbonTracker CT2016; Peters et al., 2007
[9]CASA-GFED3; van der Werf et al., 2004; 2006; 2010

Table 2: Summary of the different OSSEs conducted during this work.

Experiment (# of OSSEs)	OCO-2 XCO_2 Mode	Prior NEE Model	NEE Uncertainty
Variable Prior NEE (4)	LN + LG	All[1]	Multi-Model SD[2]
Variable Prior NEE (4)	OG	All[1]	Multi-Model SD[2]
Variable Prior Uncert. (2)	LN + LG	CASA-GFED	Uniform 10%/100%

[1] NASA-CASA, CASA-GFED, SiB-4 and LPJ

[2] SD = standard deviation

Table 3: Data corresponding to Fig. 6. Seasonally-averaged NEE (PgC yr^{-1}) averaged over the 11 TransCom-3 land regions (refer to Fig. 1) for the MsTMIP ("truth"), multi-model prior mean and multi-model posterior mean (PgC yr^{-1}). The differences between the prior and posterior model NEE values are presented as SD (1σ) and range. Prior model values are presented in standard font and posterior estimates are in bold. Seasons are represented as Winter (W): December-February, Spring (Sp): March-May, Summer (Su): June-August and Fall (F): September-November. The synthetic observations in these OSSE simulations correspond to the OCO-2 LN+LG observing modes.

	NEE: Truth				NEE: Mean								NEE: Standard Deviation								NEE: Range							
Region*	W	Sp	Su	F	W		Sp		Su		F		W		Sp		Su		F		W		Sp		Su		F	
1	1.1	-0.2	-2.8	0.7	1.1	**1.0**	0.4	**0.3**	-3.4	**-2.7**	1.3	**0.9**	0.5	**0.4**	0.5	**0.1**	0.8	**0.2**	0.5	**0.1**	1.2	**0.9**	1.0	**0.3**	1.9	**0.5**	1.2	**0.2**
2	1.5	-1.5	-2.3	0.0	1.9	**1.6**	-1.0	**-1.6**	-3.2	**-2.1**	0.6	**-0.2**	1.1	**0.3**	1.3	**0.1**	2.0	**0.2**	0.8	**0.1**	2.3	**0.6**	3.2	**0.2**	4.3	**0.4**	1.6	**0.2**
3	-0.6	-0.2	-1.4	-1.3	0.4	**-0.8**	0.6	**0.2**	-0.7	**-1.2**	0.1	**-1.3**	0.1	**0.1**	0.8	**0.2**	1.4	**0.0**	2.6	**0.1**	0.2	**0.1**	1.8	**0.3**	3.1	**0.1**	5.9	**0.2**
4	-1.5	-0.4	0.7	-0.4	-1.1	**-1.3**	-0.1	**-0.4**	0.6	**0.7**	0.0	**-0.1**	0.9	**0.1**	0.4	**0.2**	0.8	**0.1**	0.9	**0.1**	2.0	**0.1**	0.9	**0.5**	1.9	**0.2**	2.0	**0.3**
5	1.3	1.0	-1.9	-2.0	0.7	**0.9**	0.6	**0.4**	-0.8	**-1.7**	-1.4	**-2.0**	1.0	**0.2**	0.8	**0.1**	0.9	**0.1**	1.2	**0.2**	2.3	**0.5**	1.6	**0.3**	2.0	**0.2**	3.0	**0.5**
6	-2.4	-1.6	1.2	1.2	-0.9	**-1.9**	-1.1	**-1.8**	0.3	**0.8**	0.7	**1.2**	0.5	**0.2**	1.0	**0.1**	1.2	**0.2**	0.7	**0.1**	1.2	**0.3**	2.2	**0.2**	2.6	**0.5**	1.7	**0.2**
7	1.2	1.0	-4.6	1.2	1.5	**1.2**	0.9	**0.9**	-5.6	**-4.8**	2.0	**1.3**	0.9	**0.7**	1.0	**0.1**	1.6	**0.1**	0.6	**0.2**	1.8	**1.4**	2.2	**0.3**	3.3	**0.2**	1.3	**0.6**
8	1.4	0.0	-1.9	-0.4	1.4	**1.3**	-1.0	**-0.2**	-2.3	**-2.3**	0.1	**-0.7**	1.3	**0.3**	0.9	**0.1**	2.5	**0.2**	1.7	**0.1**	3.0	**0.6**	2.1	**0.3**	5.7	**0.5**	3.7	**0.2**
9	-0.1	0.4	-0.3	-0.5	0.1	**0.3**	0.0	**0.6**	-0.4	**0.1**	-0.5	**-0.4**	0.4	**0.2**	0.4	**0.1**	0.4	**0.3**	0.8	**0.0**	0.8	**0.5**	0.7	**0.2**	0.8	**0.5**	1.9	**0.1**
10	-0.6	-0.6	-0.2	-0.7	-0.1	**-0.6**	0.0	**-0.7**	0.1	**-0.4**	-0.1	**-0.8**	0.4	**0.1**	0.3	**0.1**	0.3	**0.1**	0.6	**0.1**	0.9	**0.2**	0.6	**0.2**	0.7	**0.3**	1.2	**0.3**
11	2.8	-1.7	-3.2	1.6	2.3	**2.6**	-0.9	**-1.2**	-3.7	**-3.1**	1.6	**1.3**	0.4	**0.6**	1.2	**0.2**	1.5	**0.1**	0.6	**0.1**	0.9	**1.3**	2.5	**0.5**	3.5	**0.3**	1.5	**0.3**

***TransCom-3 region name and location displayed in Fig. 1.**

Deleted: S2

Deleted: S2

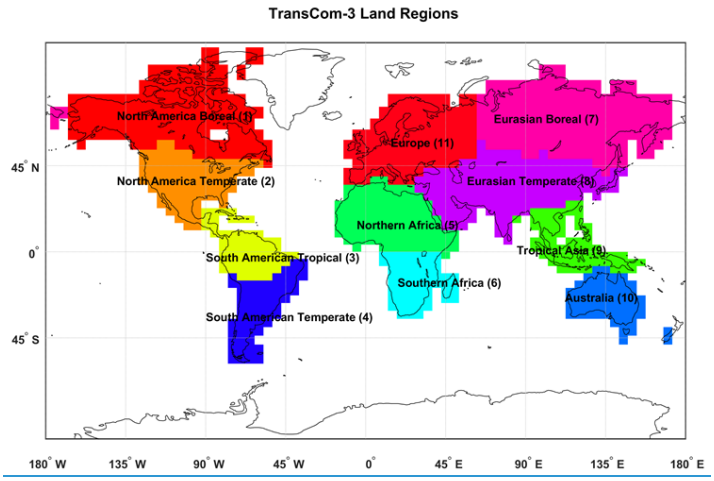

Figure 1: The TransCom-3 land region boundaries used to aggregate CO_2 fluxes for evaluation.

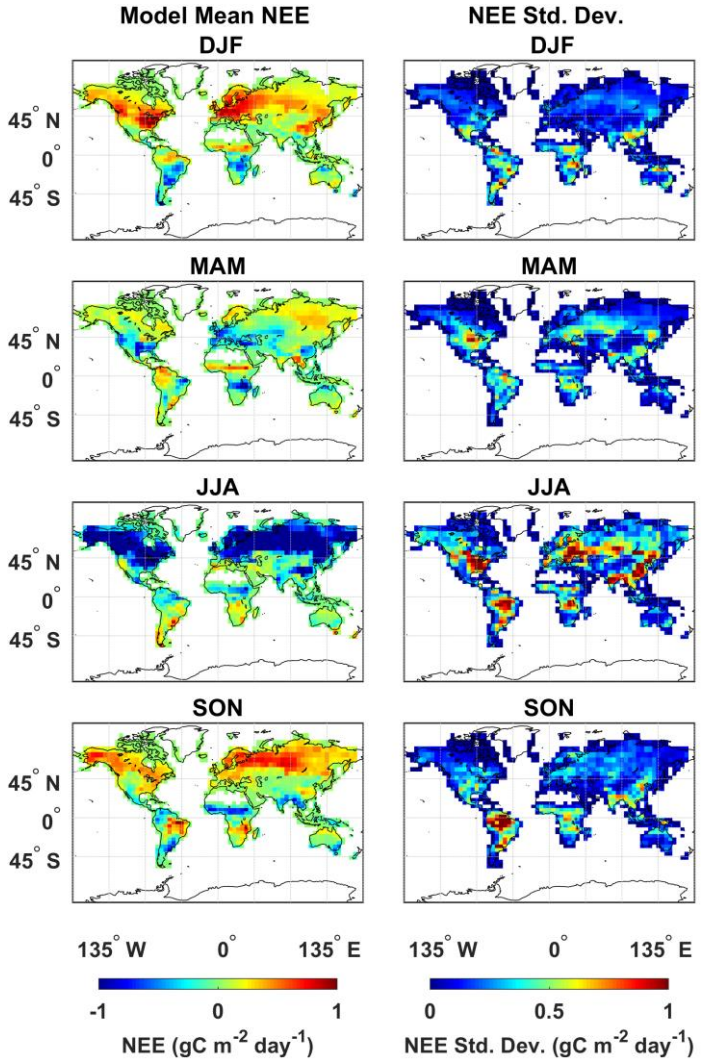

Figure 2: Prior multi-model (NASA-CASA, CASA-GFED, SiB-4 and LPJ biosphere models) seasonally-averaged NEE (gC m^{-2} day^{-1}) (left column) and NEE standard deviation (gC m^{-2} day^{-1}) (right column) for the year 2015.

Deleted: 1

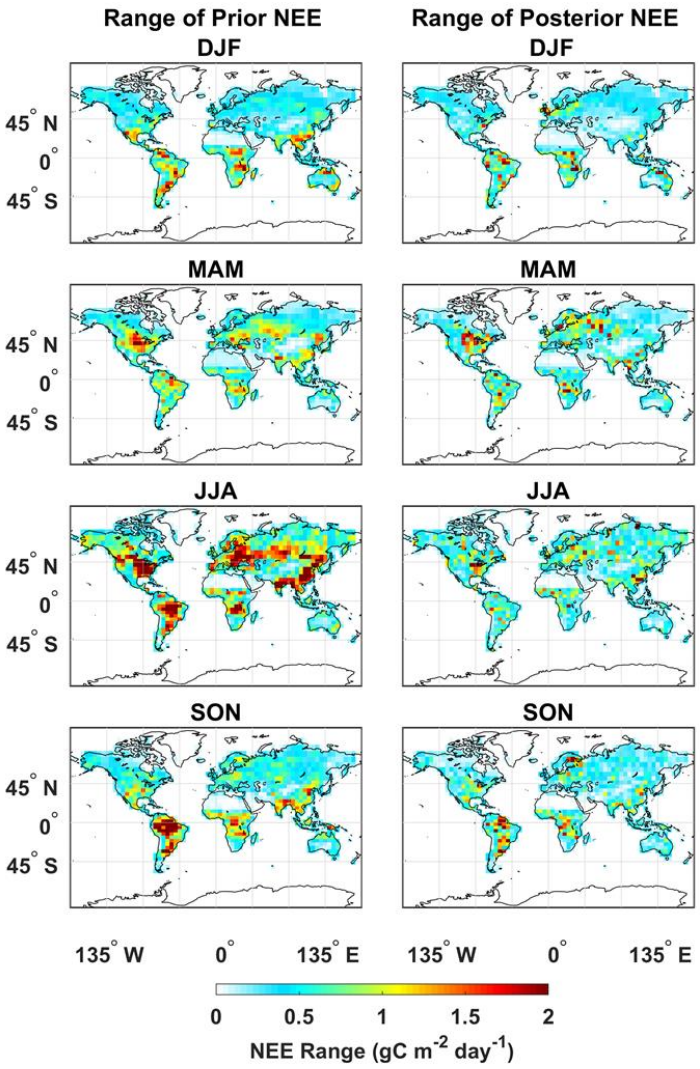

Figure 3: Seasonally-averaged NEE range (gC m^{-2} day^{-1}) of the four prior biosphere models (NASA-CASA, CASA-GFED, SiB-4 and LPJ) (left) and posterior estimates (right) from the OSSE simulations. The synthetic observations in these OSSE simulations correspond to the OCO-2 LN+LG observing modes.

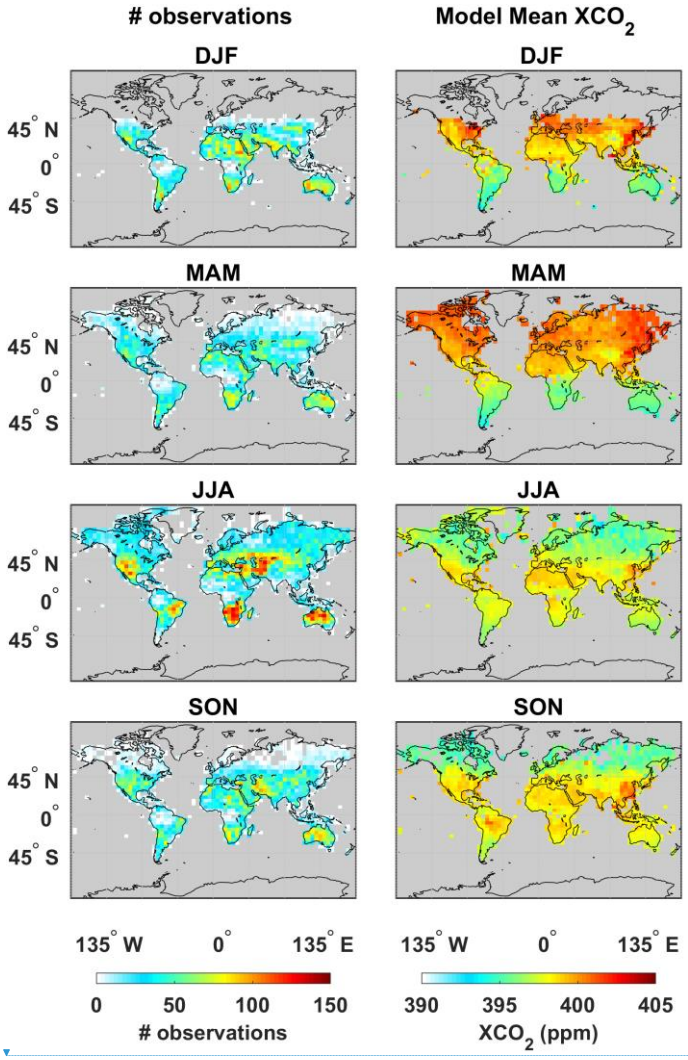

Figure 4: Total number of OCO-2 LN and LG XCO_2 observations (left column) and the corresponding seasonally-averaged multi-model (NASA-CASA, CASA-GFED, SiB-4 and LPJ biosphere models) mean GEOS-Chem-simulated prior XCO_2 (ppm) (right column) in 2015.

Deleted: ¶

Deleted: 2

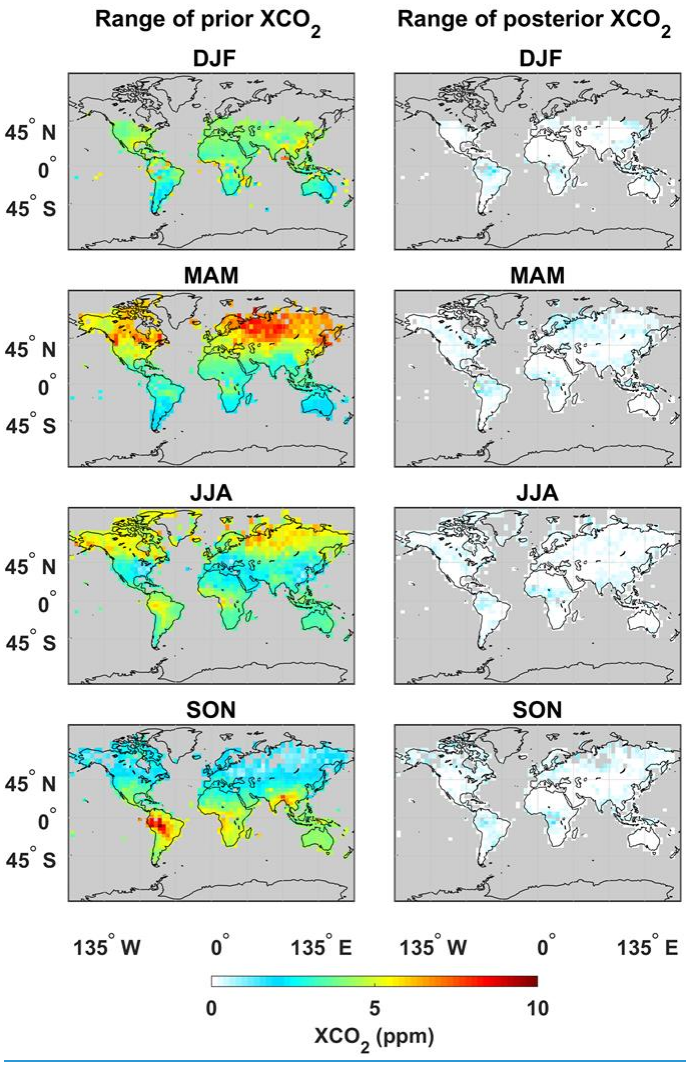

Figure 5: Seasonally-averaged XCO2 range (ppm) from GEOS-Chem forward model simulations using the four prior biosphere models (NASA-CASA, CASA-GFED, SiB-4 and LPJ) (left) and the corresponding posterior estimates (right) from the OSSE simulations. The synthetic observations in these OSSE simulations correspond to the OCO-2 LN+LG observing modes.

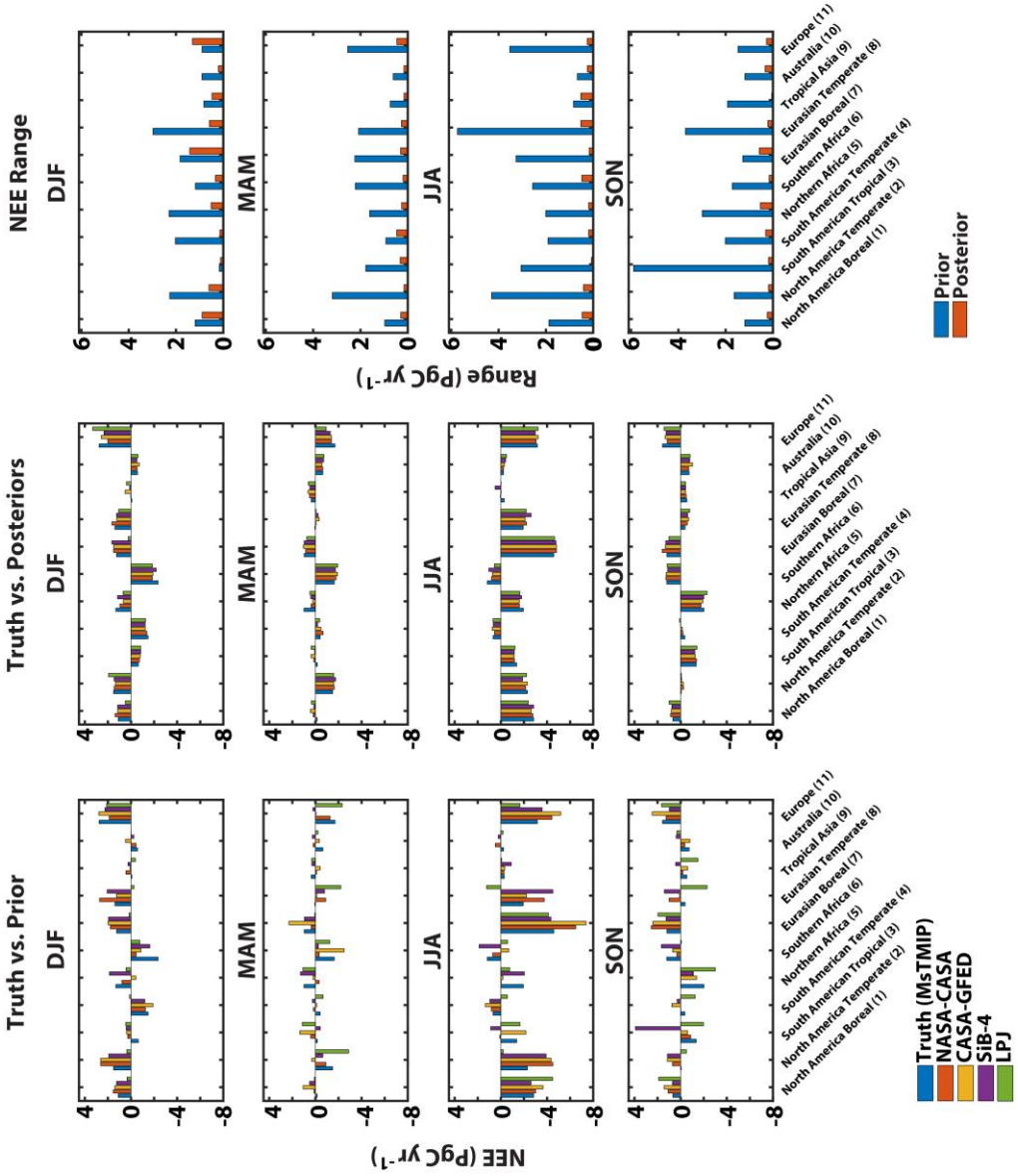

Figure 6: Seasonally-averaged NEE (PgC yr^{-1}) averaged over the 11 TransCom-3 land regions from MsTMIP ("truth") versus the prior biosphere models (NASA-CASA, CASA-GFED, SiB-4 and LPJ) (left column), posterior estimates (middle column) from the OSSE simulations and the corresponding range of prior and posterior NEE estimates (right column). The synthetic observations in these OSSE simulations correspond to the OCO-2 LN+LG observing modes. Detailed statistics of the "truth", multi-model means of prior and posterior NEE estimates, standard deviations, and ranges displayed in this figure are listed in Table 3.

Deleted: 3

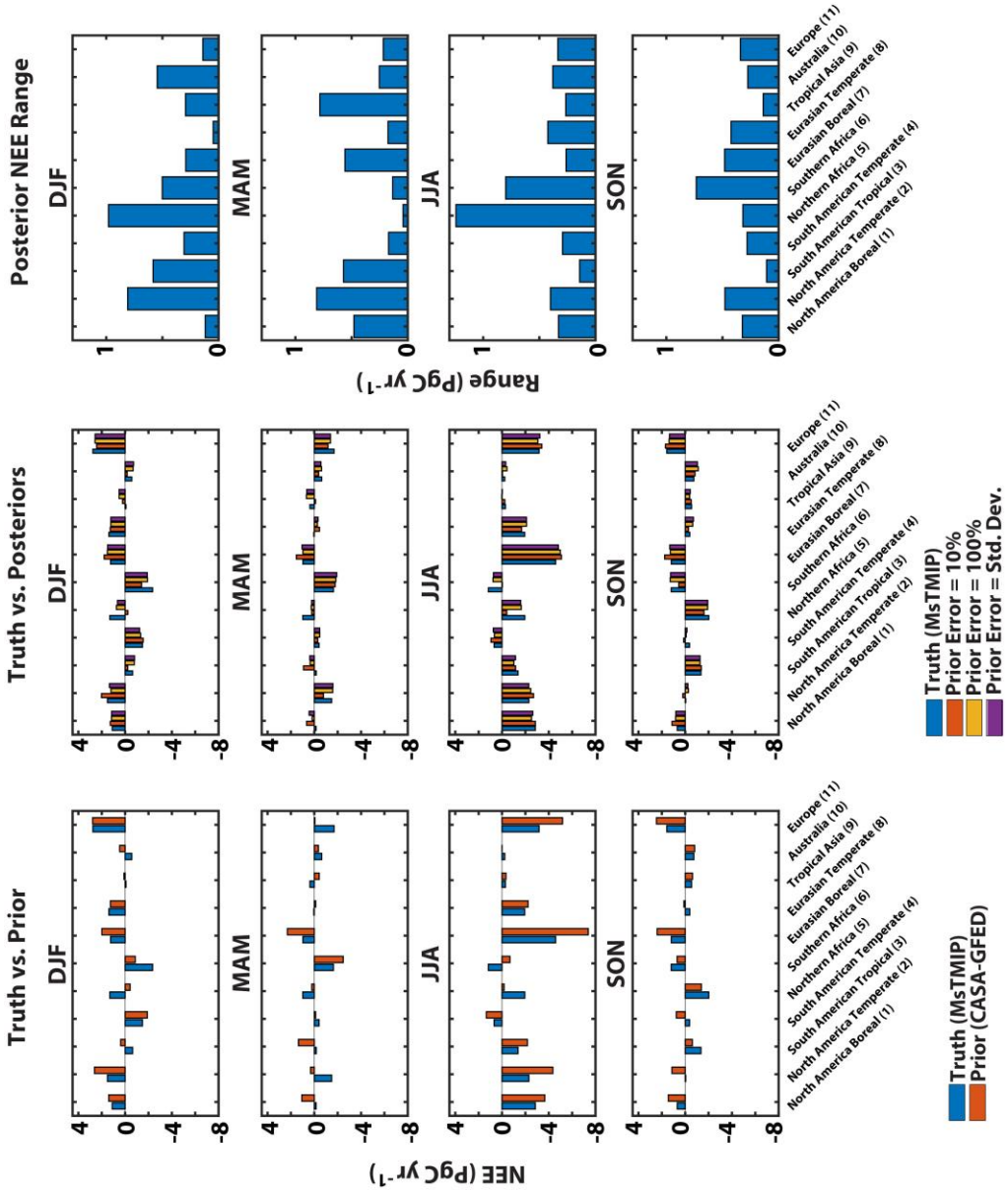

Figure 7: Seasonally-averaged NEE (PgC yr^{-1}) averaged over the 11 TransCom-3 land regions from MsTMIP ("truth") versus CASA-GFED prior biosphere model (left column), posterior estimates with the three different prior uncertainties (middle column) and the corresponding range of posterior NEE (right column). The synthetic observations in OSSE simulations correspond to the OCO-2 LN+LG observing modes. Detailed statistics of the "truth", prior, multi-model mean of posterior NEE estimates, standard deviations, and ranges displayed in this figure are listed in Table S1.

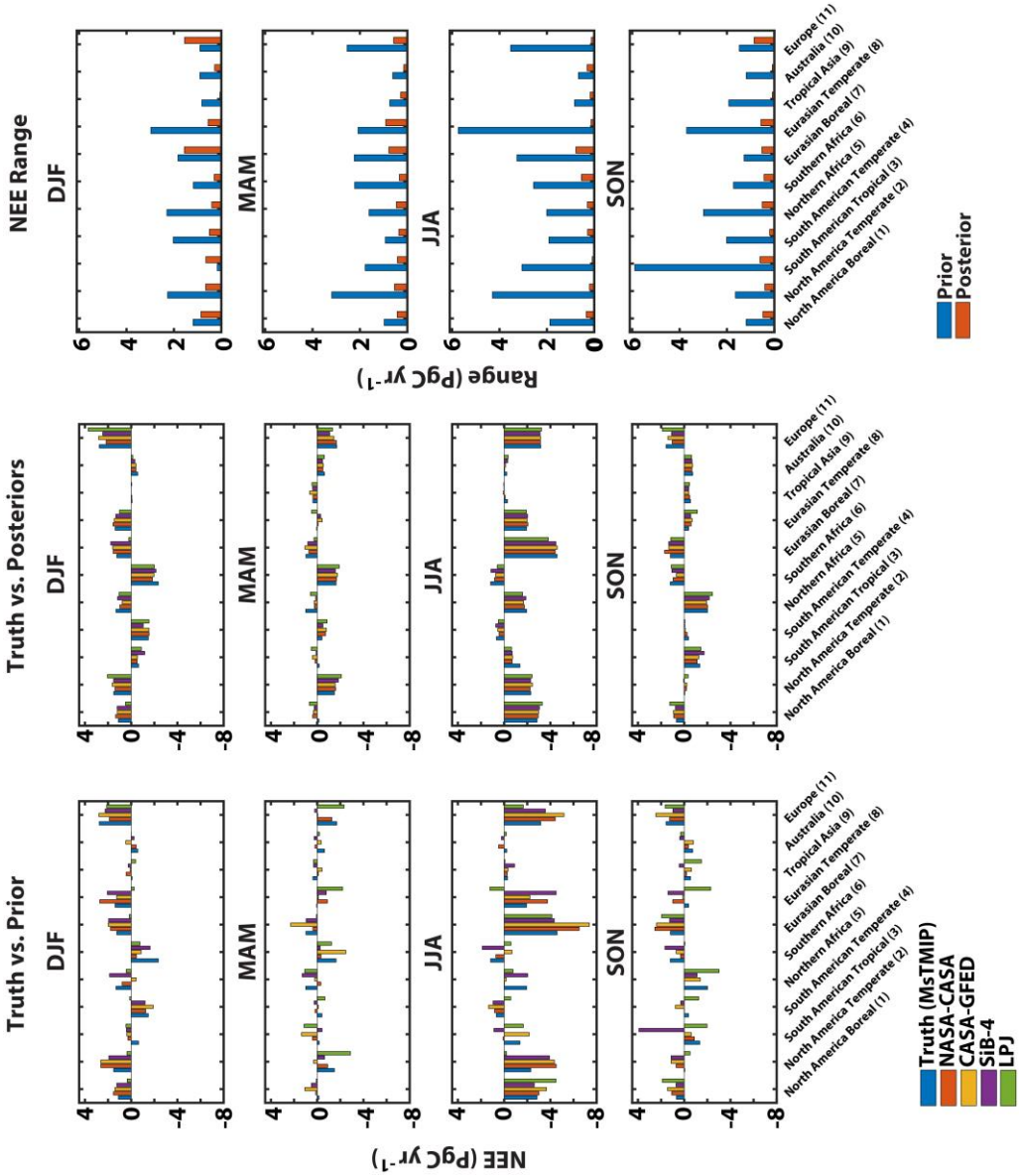

Figure 8: Seasonally-averaged NEE (PgC yr^{-1}) averaged over the 11 TransCom-3 land regions from MsTMIP ("truth") versus the prior biosphere models (NASA-CASA, CASA-GFED, SiB-4 and LPJ) (left column), posterior estimates (middle column) from the OSSE simulations and the corresponding range of prior and posterior NEE (right column). The synthetic observations in these OSSE simulations correspond to the OCO-2 OG observing mode. Detailed statistics of the "truth", multi-model means of prior and posterior NEE estimates, standard deviations, and ranges displayed in this figure are listed in Table S2.

Deleted: 5